

Quantum heat transport in condensed matter systems

Jukka P. Pekola^{1,2} and Bayan Karimi¹

¹*Pico group, QTF Centre of Excellence,
Department of Applied Physics,
Aalto University School of Science,
P.O. Box 13500, 00076 Aalto,
Finland*

²*Moscow Institute of Physics and Technology,
141700 Dolgoprudny,
Russia*

(Dated: July 28, 2021)

In this Colloquium recent advances in the field of quantum heat transport are reviewed. This topic has been investigated theoretically for several decades, but only during the past twenty years have experiments on various mesoscopic systems become feasible. A summary of the theoretical basis for describing heat transport in one-dimensional channels is first provided. Then the main experimental investigations of quantized heat conductance due to phonons, photons, electrons, and anyons in such channels are presented. These experiments are important for understanding the fundamental processes that underly the concept of a heat conductance quantum for a single channel. Then an illustration on how one can control the quantum heat transport by means of electric and magnetic fields, and how such tunable heat currents can be useful in devices is given. This lays the basis for realizing various thermal device components such as quantum heat valves, rectifiers, heat engines, refrigerators, and calorimeters. Also of interest are fluctuations of quantum heat currents, both for fundamental reasons and for optimizing the most sensitive thermal detectors; at the end of the review the status of research on this intriguing topic is given.

CONTENTS

I. Introduction	1	B. FDT for heat for a general system	18
II. Thermoelectric transport in a one-dimensional (1D) channel	2	C. Effective temperature fluctuations	19
III. Thermal conductance - measurement aspects	3	D. Progress on measuring fluctuations of heat current and entropy	19
A. Principles of measuring heat currents	3	E. Energy sensitivity of a calorimeter	20
B. Thermometry and temperature control	3	XI. Summary and outlook	21
IV. Experimental setups, background information	4	XII. Acknowledgments	22
A. Thermal conductance of a superconductor	4	References	22
B. Heat transport in tunneling	4		
C. Hamiltonian of a quantum circuit	6		
D. Quantum noise of a resistor	6		
V. Phonons	7		
VI. Electrons and fractional charges	8		
VII. Photons	10		
A. A ballistic photon channel	10		
B. Circuit limitations of the ballistic picture	11		
C. Experiments on heat mediated by microwave photons	11		
VIII. Tunable quantum heat transport	13		
A. Electronic quantum heat interferometer	14		
B. Cooling a quantum circuit	14		
IX. Quantum heat transport mediated by a superconducting qubit	15		
A. Quantum heat valve	16		
B. Thermal rectifier	17		
X. Heat current noise	17		
A. FDT for heat in tunneling	18		

I. INTRODUCTION

In this review we present advances on fundamental aspects of thermal transport in the regime where quantum effects play an important role. Usually this means dealing with atomic scale structures or low temperatures, or combination of the two. The seminal theoretical work by Pendry (1983) presented, almost 40 years ago, the important observation that a ballistic channel for any type of a carrier can transport heat at the rate given by the so-called quantum of thermal conductance G_Q . During the present millenium the theoretical ideas have developed into a plethora of experiments in systems involving phonons, electrons, photons and recently also particles obeying fractional statistics. We give an overview of these experiments backed by the necessary theoretical framework. The question whether a channel is ballistic or not, and under what conditions, is interesting as such, but it has also more practical implications. If one can

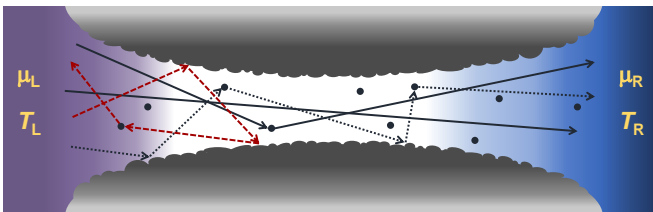


FIG. 1 Artistic representation of a generic conductor between two reservoirs. Both particles and heat are transported through. Depending on the strength and type of scattering at the impurities (dots) and walls, one can have either ballistic or diffusive transport. Here μ_i and T_i , for $i=L, R$, are the chemical potential and temperature of each reservoir on the left and right, respectively.

control the degree of ballisticity, i.e. the transmission coefficient of the channel, one can turn the heat current on and off. Such quantum heat switches, or heat valves as they are often called, will be discussed in this review as well. Furthermore heat current via a quantum element in an asymmetric structure can violate reciprocity in the sense that rectification of heat current becomes possible. The bulk of the review deals with the time average (mean) of the heat current. Yet, the fluctuations of this quantity are interesting and they provide a yardstick for the minimal detectable power and for the ultimate energy resolution of a thermal detector. We discuss such a noise and its implications in ultrasensitive detection.

The review opens after the present introductory section by a theoretical discussion of thermoelectric transport in one-dimensional channels in Section II. In Section III we present the concept and method of how to measure heat currents in general. Section IV reviews the central elements of the experimental setups. After these general sections, we move to heat transport in different physical systems: phonons in Section V, electrons and fractional charges in Section VI, and photons in Section VII including some detailed theoretical discussion in the subsections. Section VIII presents experimental results on heat control by external fields. In Section IX we move to the discussion of a superconducting qubit as a tunable element in quantum thermodynamics. Section X gives an account of both theoretical expectations and experimental status on heat current noise and associated fluctuations of effective temperature. Section XI concludes the review by a summary and outlook including prospects on useful thermal devices and some interesting physical questions related to quantum heat transport.

II. THERMOELECTRIC TRANSPORT IN A ONE-DIMENSIONAL (1D) CHANNEL

Consider two infinite reservoirs with temperature T_i and chemical potential μ_i which are connected adiabatically via a conductor as shown schematically in Fig. 1.

Here the subscripts $i=L, R$ represent the left and right, respectively. Based on Landauer theory (Landauer, 1981), (Sivan and Imry, 1986), (Butcher, 1990) the charge and energy currents, I and \mathcal{J} , between the two reservoirs (from L to R) are given for a 1D conductor by

$$I = q \sum_n \int_0^\infty \frac{dk}{2\pi} v_n(k) (\vartheta_L - \vartheta_R) \mathcal{T}_n(k)$$

$$\mathcal{J} = \sum_n \int_0^\infty \frac{dk}{2\pi} \varepsilon_n(k) v_n(k) (\vartheta_L - \vartheta_R) \mathcal{T}_n(k), \quad (1)$$

where q is the particle charge, \sum_n presents the sum over independent modes in the conductor, and $\varepsilon_n(k)$ and $v_n(k)$ indicate the energy and the velocity of the particles with wave vector k , respectively. $\mathcal{T}_n(k)$ indicates the particle transmission probability through the conductor via the channel; for ballistic transport $\mathcal{T}_n(k) \equiv 1$, and $\vartheta_{L,R}$ represents the statistical distribution functions in each reservoir. Changing the variable from wave vector to energy via the definition of the velocity $v_n(k) = \frac{1}{\hbar} \frac{\partial \varepsilon_n(k)}{\partial k}$, we have

$$I = \frac{q}{h} \sum_n \int_{\varepsilon(0)}^\infty d\varepsilon [\vartheta_L(\varepsilon) - \vartheta_R(\varepsilon)] \mathcal{T}_n(\varepsilon)$$

$$\mathcal{J} = \frac{1}{h} \sum_n \int_{\varepsilon(0)}^\infty d\varepsilon \varepsilon [\vartheta_L(\varepsilon) - \vartheta_R(\varepsilon)] \mathcal{T}_n(\varepsilon), \quad (2)$$

where $\varepsilon(0) \equiv \varepsilon$ for $k = 0$. These equations constitute the basis of thermoelectrics, with linear response for electrical and thermal conductance and for Seebeck and Peltier coefficients.

Now we solve analytically these equations for a ballistic contact $\mathcal{T}_n(\varepsilon) \equiv 1$ with the most common carriers, that is fermions and bosons. For fermions $\vartheta_i(\varepsilon) \equiv f_i(\varepsilon - \mu_i) = 1/(1 + e^{\beta_i(\varepsilon - \mu_i)})$ is the Fermi distribution function for each reservoir, with inverse temperature $\beta_i = 1/(k_B T_i)$. Note that we have taken the Fermi energy as the zero of ε , meaning that $\varepsilon(0) \rightarrow -\infty$. In this case at temperature T , with only chemical potential difference eV across the contact, the charge current is

$$I = N \frac{e}{h} \int_{-\infty}^\infty d\varepsilon [f(\varepsilon) - f(\varepsilon - eV)] = N \frac{e^2 V}{h}. \quad (3)$$

Here N replacing the sum represents the number of current carrying modes in the conductor with $q \equiv e$. The electrical conductance $G = dI/dV$ is then

$$G = Ne^2/h, \quad (4)$$

which is the famous quantization of electrical conductance. The thermal conductance for fermions can be obtained from the heat flux $\dot{Q} = \mathcal{J}$ when both reservoirs have the same chemical potential. The heat current across the ballistic contact is then

$$\dot{Q} = \frac{1}{h} \sum_n \int_{-\infty}^\infty d\varepsilon \varepsilon [f_L(\varepsilon) - f_R(\varepsilon)]. \quad (5)$$

The subtle differences between energy and heat currents are briefly discussed in Section IV.B. In this review we focus mainly on thermal conductance in equilibrium, $T_L = T_R \equiv T$, i.e. on $G_{\text{th}}(T) \equiv d\dot{Q}/dT_L|_T$. The thermal conductance is then

$$\begin{aligned} G_{\text{th}}^{(f)} &= N \frac{1}{h} \frac{1}{k_B T^2} \int_{-\infty}^{\infty} d\varepsilon \varepsilon^2 f(\varepsilon)[1 - f(\varepsilon)] \\ &= N \frac{\pi^2 k_B^2}{3h} T \equiv N G_Q, \end{aligned} \quad (6)$$

where the superscript (f) stands for fermions and

$$G_Q \equiv \frac{\pi^2 k_B^2}{3h} T \quad (7)$$

is the thermal conductance quantum. The ratio of the thermal and electrical conductances satisfies the Wiedemann-Franz law $G_{\text{th}}^{(f)}/G = \mathcal{L}T$, where the Lorenz number is $\mathcal{L} = \frac{\pi^2 k_B^2}{3e^2}$ (Ashcroft and Mermin, 1976).

We obtain the thermal conductance for bosons, $G_{\text{th}}^{(b)}$, with the same procedure but with the distribution function $\vartheta_{R,L}(\varepsilon) \equiv n_{R,L}(\varepsilon) = 1/(e^{\beta_{R,L}\varepsilon} - 1)$ in Eq. (2):

$$G_{\text{th}}^{(b)} = \frac{\hbar^2}{2\pi k_B T^2} \sum_n \int_0^\infty d\omega \frac{\omega^2 e^{\beta\hbar\omega}}{(e^{\beta\hbar\omega} - 1)^2} \mathcal{T}_n(\omega). \quad (8)$$

Here $\varepsilon = \hbar\omega$ is the energy of each boson. For a single fully transmitting channel $\mathcal{T}_n(\omega) = 1$, we then obtain again

$$G_{\text{th}}^{(b)} = G_Q. \quad (9)$$

Fermions and bosons form naturally the playground for most experimental realizations in the quantum regime. Yet the result above for a ballistic channel, $G_{\text{th}} = G_Q$, is far more general. As demonstrated in (Blencowe and Vitelli, 2000; Rego and Kirczenow, 1999), this expression is invariant even if one introduces carriers with arbitrary fractional exclusion statistics (Wu, 1994). A few years back, (Banerjee *et al.*, 2017) experimented on a fractional quantum Hall system addressing this interesting universality of thermal conductance quantum for anyons.

III. THERMAL CONDUCTANCE - MEASUREMENT ASPECTS

A. Principles of measuring heat currents

For determining thermal conductance one needs in general a measurement of local temperature. Suppose an absorber, like the one in Fig. 2(a) is heated at a constant power \dot{Q} . By continuity, the relation between \dot{Q} and temperature T of the absorber with respect to the bath temperature T_0 can often be written as

$$\dot{Q} = \mathcal{K}(T^n - T_0^n), \quad (10)$$

where \mathcal{K} and n are constants characteristic to the absorber and the process of thermalization. For instance, for the most common process in metals, coupling of absorber electrons to the phonon bath, the standard expression is $\dot{Q} = \Sigma \mathcal{V}(T^5 - T_0^5)$ (Gantmakher, 1974; Roukes *et al.*, 1985; Schwab *et al.*, 2000; Wang *et al.*, 2019; Wellstood *et al.*, 1994), where Σ is a material specific parameter and \mathcal{V} the volume of the absorber. It is often the case that the temperature difference $\delta T \equiv T - T_0$ is small, $|\delta T/T| \ll 1$, and we can linearize Eq. (10) into

$$\dot{Q} = G_{\text{th}} \delta T, \quad (11)$$

where $G_{\text{th}} = n\mathcal{K}T_0^{n-1}$ is the thermal conductance between the absorber and the bath. For the electron-phonon coupling above, we then have $G_{\text{th}}^{(\text{ep})} = 5\Sigma\mathcal{V}T_0^4$. It is worth pointing out that electron-electron relaxation in metals is fast enough to secure a well defined electron temperature (Pothier *et al.*, 1997).

For the ballistic channel discussed widely in the current manuscript, $G_{\text{th}} \equiv G_Q = \frac{\pi^2 k_B^2}{3h} T_0$, and we have for a general temperature difference exactly

$$\dot{Q} = \frac{\pi^2 k_B^2}{6h} (T^2 - T_0^2) = \frac{\pi^2 k_B^2}{3h} T_m \delta T, \quad (12)$$

where $T_m \equiv (T + T_0)/2$ is the mean temperature.

In some experiments a differential two-absorber setup is preferable (see Fig. 2(b)). This allows for measurements of the temperatures of the two absorbers, T_1 and T_2 , separately, and to determine the heat flux between the two without extra physical (wiring) connections for thermometry across the object of interest. In this case equations in this section apply if we replace T , T_0 by T_1 , T_2 , respectively. Such a setup offers more flexible calibration and sanity check options for the system, and also for tests of reciprocity (thermal rectification) by inverting the roles of source and drain, i.e., by reversing the temperature bias.

B. Thermometry and temperature control

Here we comment very briefly on thermometry and temperature control in the experiments to be reported in this paper. The control of the local temperature is typically achieved by Joule heating applied to the electronic system. But depending on the type of the reservoir, this heat is either directly acting on the quantum conductor or indirectly, e.g. via the phonon bath. The simplest heating element is a resistive on-chip wire. For heating (and local cooling), and in particular for thermometry, a hybrid normal metal-insulator-superconductor tunnel junction (NIS junction) is a common choice (Courtois *et al.*, 2014; Giazotto *et al.*, 2006; Muhonen *et al.*, 2012). We defer discussion of this technique to Section IV.B. In several experiments a simple resistive on-chip wire is

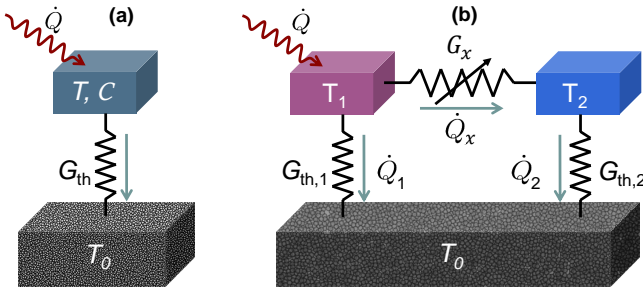


FIG. 2 Thermal models. (a) A finite-sized reservoir at temperature T and of heat capacity C coupled to a heat bath at fixed temperature T_0 via a heat link with thermal conductance G_{th} . The absorbed heat current \dot{Q} creates a temperature difference. (b) Two finite-sized absorbers each coupled to the heat bath and to each other via a potentially tunable thermal conductance G_x with the associated heat current \dot{Q}_x of the system under study.

used as a local heater. For thermometry one may use a similar wire and measure its thermal noise (Schwab *et al.*, 2000). Another option used in some recent experiments is to measure the current noise of a quantum point contact (Banerjee *et al.*, 2017; Jezouin *et al.*, 2013).

IV. EXPERIMENTAL SETUPS, BACKGROUND INFORMATION

A. Thermal conductance of a superconductor

A superconductor obeying Bardeen-Cooper-Schrieffer theory (BCS theory) (Bardeen *et al.*, 1957) forms an ideal building block for thermal experiments at low temperatures. A basic feature of a BCS-superconductor is its zero resistance, but in our context an even more important property is its essentially vanishing thermal conductance (Bardeen *et al.*, 1959). In bulk superconductors both electronic and the non-vanishing lattice thermal conductances play a role.

In small structures the exponentially vanishing thermal conductance at low temperatures can be exploited effectively to form thermal insulators that can at the same time provide perfect electrical contacts. In quantitative terms, according to the theory (Bardeen *et al.*, 1959), the ratio of the thermal conductivity $\kappa_{e,S}$ in the superconducting state and $\kappa_{e,N}$ in the normal state of the same material is given by

$$\kappa_{e,S}/\kappa_{e,N} = \int_{\Delta}^{\infty} d\epsilon \epsilon^2 f'(\epsilon) / \int_0^{\infty} d\epsilon \epsilon^2 f'(\epsilon), \quad (13)$$

where $\Delta \approx 1.76k_B T_C$ is the gap of the superconductor with critical temperature T_C . For temperatures well below T_C , i.e., for $\Delta/k_B T \gg 1$, we obtain an approximate answer for Eq. (13) as

$$\kappa_{e,S}/\kappa_{e,N} \approx \frac{6}{\pi^2} \left(\frac{\Delta}{k_B T} \right)^2 e^{-\Delta/k_B T}. \quad (14)$$

Since the normal state thermal and electrical conductivities are related by the Wiedemann-Franz law, we obtain

$$\kappa_{e,S} \approx \frac{2\Delta^2}{e^2 \rho T} e^{-\Delta/k_B T}, \quad (15)$$

where ρ is the normal state resistivity of the conductor material. As usual, for the basic case of a uniform conductor with cross-sectional area A and length ℓ , we may then associate the thermal conductance G_{th} to thermal conductivity κ as $G_{\text{th}} = (A/\ell)\kappa$.

Aluminum and niobium are the most common superconductors used in the experiments described here. In many respects, Al follows BCS-theory accurately. In particular it has been shown (Saira *et al.*, 2012a) that the density of states (DoS) at energies inside the gap is suppressed at least by a factor $\sim 10^{-7}$ leading for instance to the exponentially high thermal insulation discussed here. The measured thermal conductivity of Al follows closely Eq. (15), shown in (Feshchenko *et al.*, 2017; Peltonen *et al.*, 2010). At the same time Nb films suffer from non-vanishing subgap DoS, leading to power-law thermal conductance in T , i.e. poor thermal insulation at the low temperature regime. In conclusion of this subsection we want to emphasize that Al is a perfect thermal insulator at $T \lesssim 0.3T_C$, except in the immediate contact with a normal metal leading to inverse proximity effect; this proximity induced thermal conductivity affects typically only within few hundred nm distances from a clean normal metal contact (Peltonen *et al.*, 2010).

B. Heat transport in tunneling

One central element in this review is a tunnel junction between two electrodes L (left) and R (right). The charge and heat currents through the junction can be obtained by perturbation theory where the coupling Hamiltonian between the electrodes is written as the tunnel Hamiltonian (Bruus and Flensberg, 2004)

$$\hat{H}_c = \sum_{l,r} (t_{lr} \hat{a}_l^\dagger \hat{a}_r + t_{lr}^* \hat{a}_l \hat{a}_r^\dagger). \quad (16)$$

Here t_{lr} is the tunneling amplitude, and $\hat{a}_{l(r)}^\dagger$ and $\hat{a}_{l(r)}$ are the creation and annihilation operators for electrons in the left (right) electrode, respectively.

To have the expression for number current from R to L one first obtains operator for it as $\hat{N}_L = \frac{i}{\hbar} [\hat{H}_c, \hat{N}_L]$, where $\hat{N}_L = \sum_l \hat{a}_l^\dagger \hat{a}_l$ is the operator for the number of electrons in L. Then one can write the charge current operator as $\hat{I} = -e\hat{N}_L$. In order to obtain the expectation value of the current that is measured in an experiment, $I \equiv \langle \hat{I} \rangle$, we employ linear response theory (Kubo formula (Kubo, 1957)) on the corresponding current operator, where $I = -i/\hbar \int_{-\infty}^0 dt' \langle [\hat{I}(0), \hat{H}_c(t')] \rangle_0$, with $\langle \cdot \rangle_0$

the expectation value in the unperturbed state. Assuming that the averages are given by the Fermi distributions in each lead, we have at voltage bias V

$$I = \frac{1}{eR_T} \int d\epsilon n_L(\tilde{\epsilon})n_R(\epsilon)[f_L(\tilde{\epsilon}) - f_R(\epsilon)], \quad (17)$$

where $\tilde{\epsilon} = \epsilon - eV$. Here the constant prefactor includes the inverse of the resistance R_T of the junction such that $1/R_T = 2\pi|t|^2\nu_L(0)\nu_R(0)e^2/\hbar$, with $|t|^2 = |t_r|^2 = \text{constant}$, and $\nu_L(0), \nu_R(0)$ the density of states (DoS) in the normal state at Fermi energy in the left and right electrodes, respectively. Under the integral, $n_L(\epsilon), n_R(\epsilon)$ are the normalized (by $\nu_L(0), \nu_R(0)$, respectively) energy dependent DoSes, and $f_L(\epsilon), f_R(\epsilon)$ the corresponding energy distributions that are Fermi-Dirac distributions for equilibrium electrodes.

For heat current we use precisely the same procedure but now for the operator of energy of the left electrode $\hat{H}_L = \sum_l \epsilon_l \hat{a}_l^\dagger \hat{a}_l$, instead of the number operator, where ϵ_l is the energy of a single particle state in L. Then we find the expectation value of the heat current out from L electrode, $\dot{Q}_L = -\langle \dot{H}_L \rangle$ as

$$\dot{Q}_L = \frac{1}{e^2 R_T} \int d\epsilon \tilde{\epsilon} n_L(\tilde{\epsilon})n_R(\epsilon)[f_L(\tilde{\epsilon}) - f_R(\epsilon)]. \quad (18)$$

Here we may briefly comment on the relation of energy and heat currents, \mathcal{J} and \dot{Q} introduced in Section II. Inserting $\tilde{\epsilon} = \epsilon - eV$, we find immediately $\dot{Q}_L = \mathcal{J} - IV$, where $\mathcal{J} \equiv (e^2 R_T)^{-1} \int d\epsilon \epsilon n_L(\tilde{\epsilon})n_R(\epsilon)[f_L(\tilde{\epsilon}) - f_R(\epsilon)]$. Writing the equation for the heat from the right electrode in analogy to Eq. (18), we find $\dot{Q}_R = -\mathcal{J}$. Thus we have $\dot{Q}_L + \dot{Q}_R = -IV$, which presents energy conservation: the total power taken from the source goes into heating the two electrodes. This is natural since in steady state work equals heat, as the internal energy of the system is constant.

As the most basic example of both the electrodes being normal metal (NIN junction, I for insulator), we have $n_L(\epsilon) = n_R(\epsilon) = 1$. Equations (17) and (18) then yield under quite relaxed conditions $I = V/R_T$ and $\dot{Q}_L = -\frac{V^2}{2R_T}$, i.e. the junction is ohmic and the Joule power is dissipated equally to the two electrodes.

Another important example is a normal-superconductor junction (NIS junction, L=N, R=S), Fig. 3. Its usefulness in thermometry (see Fig. 3(a)) is based on the superconducting gap Δ that leads to non-linear, temperature dependent current-voltage characteristics. This feature probes the temperature of the normal side of the contact. Such a temperature dependence is universal, $d \ln(I/I_0)/dV = e/(k_B T)$, where $I_0 = \sqrt{\pi \Delta k_B T / 2} / (e R_T)$, making NIS a primary thermometer in principle. This is strictly speaking true only for an ideal junction with low transparency. Therefore the common practice is to use it as a secondary thermometer (Lounasmaa, 1974), meaning that one

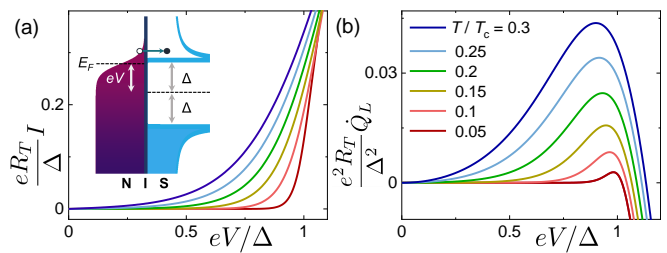


FIG. 3 Properties of an NIS tunnel junction. The inset in (a) shows the energy diagram of a biased by voltage V junction between a normal metal (N) and superconducting (S) electrode connected via an insulating (I) barrier. Due to the BCS gap Δ in S, transport is blocked at $eV \ll \Delta$. At a voltage close to the gap value, as in the figure, electrons at the highest energy levels can tunnel to the superconductor as shown, leading to both non-vanishing charge current and cooling of N. The main frame of (a) shows calculated current-voltage curves at different values of $T/T_c = 0.05 - 0.3$ from bottom to top (for both panels): at these subgap voltages the junction provides a sensitive thermometer. (b) presents similarly calculated power \dot{Q}_L versus V curves, demonstrating cooling of N at $eV \lesssim \Delta$. At higher voltages $eV \gg \Delta$, \dot{Q}_L becomes negative, meaning it serves as a Joule heater of N.

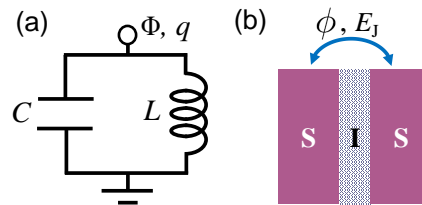


FIG. 4 Central elements of superconducting quantum devices. (a) LC circuit with flux Φ and charge q . (b) Josephson junction with phase difference ϕ and Josephson energy E_J .

measures a thermometric response of it near equilibrium, for instance the voltage at a small fixed current, against the independently measured temperature of the cryostat (heat bath). The other important feature of the NIS junction lies in its thermal properties. When biased at a voltage of about Δ/e , heat is carried away from the N side (and S is heated), i.e., it acts as a refrigerator (see Fig. 3(b)). At $V \gg \Delta/e$ the junction provides usual Joule heating. This is how a NIS junction can be used both as a cooler and heater of a mesoscopic reservoir. Numerically calculated current-voltage and cooling power characteristics, together with a schematic energy diagram have been depicted in the figure. The main characteristics of a NIS junction, based on analytical approximations at low temperatures are: $I \approx I_0 e^{-\Delta/k_B T}$ at voltages below the gap, and the maximal cooling of normal metal at $eV \approx \Delta$ is $\dot{Q}_L^{\max} \approx +0.59(\Delta^2/e^2 R_T)(k_B T/\Delta)^{3/2}$.

Microrefrigeration by electron transport is a technique that has been reviewed elsewhere (Courtois *et al.*, 2014; Giazotto *et al.*, 2006; Muhonen *et al.*, 2012). For an in-

terested reader, the following non-exhaustive list of original references on the topic besides the mentioned review articles could be recommended: (Clark *et al.*, 2004; Feshchenko *et al.*, 2014; Kuzmin *et al.*, 2004; Leivo *et al.*, 1996; Nahum *et al.*, 1994; Nguyen *et al.*, 2013; Prance *et al.*, 2009).

C. Hamiltonian of a quantum circuit

Another key element in our context is a harmonic oscillator, and in some cases a non-linear quantum oscillator, usually in form of a Josephson junction (Tinkham, 2004). To avoid dissipation the linear harmonic oscillator in a circuit is commonly made of a superconductor, often in form of a coplanar wave resonator (Krantz *et al.*, 2019). The Hamiltonian of such an LC -oscillator, shown in Fig. 4(a) is composed of the kinetic $q^2/(2C)$ and potential $\Phi^2/(2L)$ energies, respectively, where q is the charge on the capacitor and Φ the flux of the inductor.

The charge is the conjugate momentum to flux as $q = C\dot{\Phi}$, and the total Hamiltonian is then

$$\hat{H} = \frac{\hat{q}^2}{2C} + \frac{\hat{\Phi}^2}{2L}, \quad (19)$$

i.e. that of a harmonic oscillator, with \hat{q} and $\hat{\Phi}$ as charge and flux operators, respectively. Introducing the creation \hat{c}^\dagger and annihilation \hat{c} operators such that $[\hat{c}, \hat{c}^\dagger] = 1$, we have

$$\hat{\Phi} = \sqrt{\frac{\hbar Z_0}{2}}(\hat{c} + \hat{c}^\dagger), \quad \hat{q} = -i\sqrt{\frac{\hbar}{2Z_0}}(\hat{c} - \hat{c}^\dagger), \quad (20)$$

yielding the standard harmonic oscillator Hamiltonian

$$H = \hbar\omega_0(\hat{c}^\dagger\hat{c} + \frac{1}{2}), \quad (21)$$

where $\omega_0 = 1/\sqrt{LC}$, and $Z_0 = \sqrt{L/C}$ are the (angular) frequency and impedance of the oscillator.

For a Josephson tunnel junction, shown in Fig. 4(b), the Josephson relations (Josephson, 1962) are

$$\hbar\dot{\phi} = 2eV, \quad I = I_c \sin \phi, \quad (22)$$

where ϕ is the phase difference across the junction related to flux by $\phi = (2e/\hbar)\Phi$. In the second Josephson relation, I is the current through the junction. The sinusoidal current-phase relation applies strictly for a tunnel junction, with critical current I_c . For different types of weak links, sinusoidal dependence does not necessarily hold (Tinkham, 2004). The energy stored in the junction (=work done by the source) is then obtained for a current biased case from $I = \partial E/\partial\Phi$ as

$$E = \int^\Phi I d\Phi = -E_J \cos \phi. \quad (23)$$

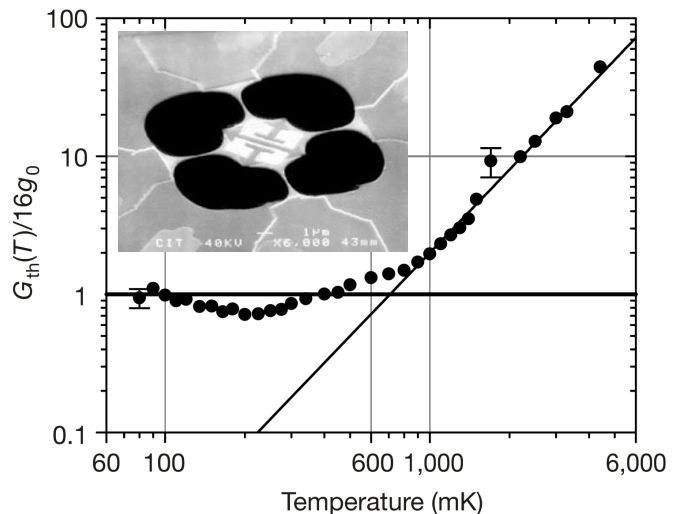


FIG. 5 View of the suspended structure of (Schwab *et al.*, 2000) for measuring quantized thermal conductance. (Inset) In the center, $4 \times 4 \mu\text{m}^2$ phonon cavity is patterned from the membrane; the bright areas on the central membrane are Au-thin-film transducers connected to Nb-thin-film leads on top of phonon waveguides. The membrane has been completely removed in the dark regions. (main panel) Temperature dependence of the measured thermal conductance normalized by $16G_Q$ ($16g_0$). Adapted from (Schwab *et al.*, 2000).

This constitutes the Josephson part of the Hamiltonian, also called \hat{H}_J . For small values of ϕ , ignoring the constant part, we have

$$E \simeq \frac{\Phi^2}{2L_J}, \quad (24)$$

where $L_J = \hbar/(2eI_c)$ is the Josephson inductance. Therefore, in the “linear regime” a Josephson junction can be considered as a harmonic oscillator such that Eqs. (19)-(21) apply with L replaced by L_J . Yet the actual non-linearity of a Josephson junction makes it an invaluable component in quantum information processing and in quantum thermodynamics.

A magnetic flux tunable Josephson junction, for instance in form of two parallel junctions with a superconducting loop in between, is the renowned superconducting quantum interference device (SQUID) to be discussed in later sections.

D. Quantum noise of a resistor

The quantum noise of a resistor is an important quantity as it determines the heat emission and absorption in form of thermal excitations. In later sections it becomes obvious how this noise yields the Joule power in a circuit.

Consider that the resistor in the quantum circuit is formed of a collection of harmonic oscillators with ladder operators \hat{b}_i and \hat{b}_i^\dagger with frequencies ω_i . The phase

operator in the interaction picture reads

$$\phi(t) = \sum_i \lambda_i (\hat{b}_i e^{-i\omega_i t} + \hat{b}_i^\dagger e^{i\omega_i t}), \quad (25)$$

with coefficients λ_i . The voltage fluctuations are related to phase as $v(t) = \frac{\hbar}{e} \dot{\phi}(t)$

$$v(t) = i \frac{\hbar}{e} \sum_i \lambda_i \omega_i (\hat{b}_i^\dagger e^{i\omega_i t} - \hat{b}_i e^{-i\omega_i t}). \quad (26)$$

Then the spectral density of voltage noise $S_v(\omega) = \int_{-\infty}^{\infty} dt e^{i\omega t} \langle v(t)v(0) \rangle$ is given by

$$S_v(\omega) = \frac{2\pi\hbar^2}{e^2} \int_0^\infty d\Omega \nu(\Omega) \lambda(\Omega)^2 \Omega^2 \left\{ [1 + n(\Omega)]\delta(\omega - \Omega) + n(\Omega)\delta(\omega + \Omega) \right\}, \quad (27)$$

where $\nu(\Omega)$ is the oscillator density of states. Now we consider both positive and negative frequencies, which correspond to quantum emission and absorption processes. For positive frequencies only the first term survives as

$$S_v(\omega) = \frac{2\pi\hbar^2}{e^2} \nu(\omega) \lambda(\omega) \omega^2 [1 + n(\omega)] \quad (28)$$

Considering similarly the negative frequencies, we find

$$S_v(-\omega) = e^{-\beta\hbar\omega} S_v(\omega), \quad (29)$$

which is the famous *detailed balance condition*.

We know that the classical Johnson-Nyquist noise (Johnson, 1928; Nyquist, 1928) of a resistor at $k_B T \gg \hbar\omega$ reads

$$S_v(\omega) = 2k_B T R. \quad (30)$$

This is the classical fluctuation-dissipation theorem (FDT (Callen and Welton, 1951)) applied to the resistor. In this limit by using Taylor expansion, we have $(1 - e^{-\beta\hbar\omega})^{-1} \simeq (\beta\hbar\omega)^{-1}$, so that using Eq. (28) we have connection between the oscillator properties and the physical resistance as (Karimi and Pekola, 2021)

$$\lambda_i^2 = \frac{Re^2}{\pi\hbar\nu(\omega_i)\omega_i}. \quad (31)$$

Substituting this result in Eq. (27), we obtain at all frequencies

$$S_v(\omega) = 2R \frac{\hbar\omega}{1 - e^{-\beta\hbar\omega}}. \quad (32)$$

V. PHONONS

Quantized thermal conductance was demonstrated experimentally for the first time by (Schwab *et al.*, 2000). In

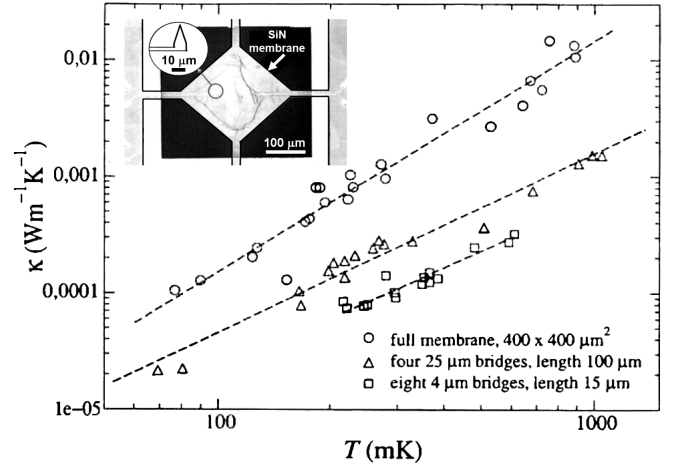


FIG. 6 Thermal conductivity κ of a 200 nm-thick silicon nitride membrane measured in three different geometries as a function of membrane temperature. Dashed lines present the fitted functions: $\kappa \simeq 14.5T^{1.98} \text{ mWm}^{-1}\text{K}^{-1}$ for full membrane, $\kappa \simeq 1.58T^{1.54} \text{ mWm}^{-1}\text{K}^{-1}$ and $\kappa \simeq 0.57T^{1.37} \text{ mWm}^{-1}\text{K}^{-1}$ for 25 μm and 4 μm wide bridges, respectively, where T is expressed in K. The data of $400 \times 400 \mu\text{m}^2$ full membrane and 25 μm -wide bridge are presented in (Leivo and Pekola, 1998) while the one for 4 μm -wide bridge is unpublished (Leivo, 1999). The corresponding thermal conductance $G_{\text{th}} = \kappa A/L$ for one bridge with area A and length L at $T = 0.1 \text{ K}$ for both 25 μm and 4 μm are $2.3 \times 10^{-12} \text{ W/K}$ and $1.3 \times 10^{-12} \text{ W/K}$ that give $N \simeq 24$ and $N \simeq 14$, respectively, assuming fully ballistic channels. Adapted from (Leivo and Pekola, 1998; Leivo, 1999).

their setup, as shown in the inset of Fig. 5, the "phonon cavity" consists of a $4 \times 4 \mu\text{m}^2$ block of silicon nitride membrane with 60 nm thickness suspended by four legs of equal thickness. Each leg has catenoidal waveguide shape whose diameter at the narrowest point is less than 200 nm. This waveguide shape as a 1D channel is the ideal profile to achieve unit transmissivity between the suspended cavity and the bulk reservoir (Rego and Kirichenow, 1998). Two Au-film resistors with 25 nm thickness were patterned on the suspended central block; one of them serves to apply the Joule heating to generate the temperature gradient along the legs and the other one worked as a thermometer to measure the phonon cavity temperature. The electron temperature of the resistor was measured by a low noise amplifier (dc SQUID) operating with nearly quantum-limited energy sensitivity by measuring the electrical Johnson noise of the resistor.

The measurement of (Schwab *et al.*, 2000) probes the thermal conductance by phonons across the four silicon nitride bridges as a function of bath temperature. These data are shown in the main frame of Fig. 5. The result exhibits the usual phononic thermal conductance, $\propto T^3$, at temperatures above 1 K. Below this temperature there is a rather abrupt leveling off of G_{th} to the value $16G_Q$ (here the notation is such that $g_0 \equiv G_Q$). The authors

argue that the coefficient 16 arises from the trivial factor 4 due to four independent bridges in the structure and the less trivial factor 4 due to four possible acoustic vibration modes of each leg in the low temperature limit: one longitudinal, one torsional, and two transverse modes. In later theoretical works the somewhat meandering behavior of $G_{\text{th}}/G_{\text{Q}}$ below the crossover temperature was explained to arise from remaining scattering of phonons in the bridges, i.e. from non-ballistic transport, whose effect is expected to get weaker in the low temperature limit (Santamore and Cross, 2001).

Over the years, there have been a few other experiments on thermal conductance by phonons in restricted geometries. The one by Leivo (Leivo and Pekola, 1998; Leivo, 1999; Manninen *et al.*, 1997) employed 200 nm-thick silicon nitride membranes in various geometries (see Fig. 6). The experiments were performed by applying Joule heating on a central membrane in an analogous way as in the experiment of (Schwab *et al.*, 2000), and the resulting temperature change to obtain the thermal conductance was then read out by measuring the temperature dependent conductance of NIS probes processed on top of the same membrane. In this case the wiring running along the bridges was made of aluminum which is known to provide close to perfect thermal isolation at temperatures well below the superconducting transition at $T_{\text{C}} \approx 1.4$ K, see Section IV.A. In general, there are many conduction channels in the wide bridges, as demonstrated in the figure caption. Yet this number for a single $w = 4 \mu\text{m}$ wide bridge is $N = 14$ at $T = 100$ mK, which is already in the same ballpark as the prediction of $N = 4$ of (Rego and Kirczenow, 1998). Naturally the ballisticity of these $15 \mu\text{m}$ long bridges is unknown though. Yet these experiments provide evidence of thermal conductance close to the quantum limit.

The experiment of (Schwab *et al.*, 2000) was followed by several measurements in different temperature ranges and materials. Experiments on GaAs phonon bridges of sub- μm lateral dimensions were earlier performed at temperatures above 1 K (Tighe *et al.*, 1997) and later down to 25 mK bath temperature (Yung *et al.*, 2002). The latter experiment measuring the temperature of the GaAs platform in the middle using NIS tunnel junctions demonstrated Debye thermal conductance at $T \gg 100$ mK, but tended to follow the expected quantum thermal conductance at the lowest temperatures. In the more recent experiments by (Tavakoli *et al.*, 2017, 2018) the measurement on sub-micron wide silicon nitride bridges was made differential in the sense that there was no need to add superconducting leads on these phonon-conducting legs. The results at the lowest temperatures of ~ 0.1 K fall about one order of magnitude below the quantum value, and the temperature dependence of thermal conductance is close to T^2 . The authors of (Tavakoli *et al.*, 2017, 2018) propose non-ballistic transmission in their bridges to be the origin of their results. Finally experiments by (Zen

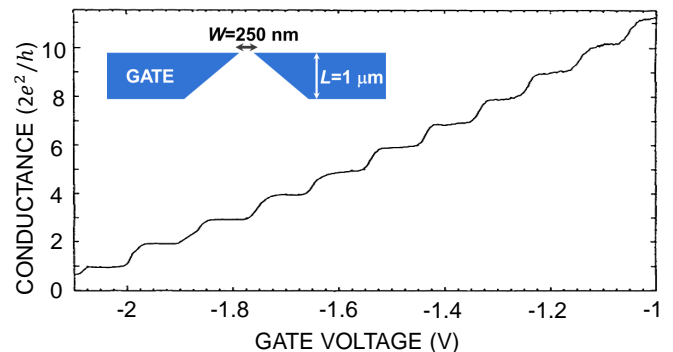


FIG. 7 Measured quantized conductance of a point contact in a two-dimensional electron gas as a function of gate voltage. The conductance demonstrates plateaus at multiples of $2e^2/h$. The layout of the point contact is shown schematically in the inset. Adapted from (van Wees *et al.*, 1988).

et al., 2014) demonstrate that thermal conductance can be suppressed strongly even in two-dimensions by proper patterning of the membranes into a nanostructured periodic phononic crystal.

VI. ELECTRONS AND FRACTIONAL CHARGES

Charged particles play a special role in assessing quantum transport properties, since they provide a straightforward access to both particle number current and heat current. For instance, in the case of electrons, we can count the carriers by measuring directly the charge current and the associated conductance. When the mean free path of the carriers is much larger than the physical dimensions of the contact, transport can become ballistic. According to Eq. (4), the electrical conductance then assumes only integer multiple values of elementary conductance quantum. The very first experiments on quantized conductance of a point contact in a GaAs-AlGaAs two-dimensional high mobility electron gas (2DEG) heterostructures were performed by (van Wees *et al.*, 1988; Wharam *et al.*, 1988). In (van Wees *et al.*, 1988) the point contact was formed by a top metallic gate with a width $W \simeq 250$ nm opening in a tapered geometry to form a voltage-controlled narrow and short channel in the underlying electron gas. The layout of the gate electrode is shown in the inset of Fig. 7. At negative gate voltages electrons are repelled under the gate and the width of the channel for carriers is $\lesssim 100$ nm which is well below the mean free path of $l \simeq 8.5 \mu\text{m}$. The measured conductance of the point contact shown in Fig. 7 exhibits well defined plateaus at the expected positions $N2e^2/h$ as a function of applied gate voltage (van Wees *et al.*, 1988). The factor 2 with respect to Eq. (4) arises from spin degeneracy.

Thirty years after the experiments on quantized electrical conductance by electrons (van Wees *et al.*, 1988;

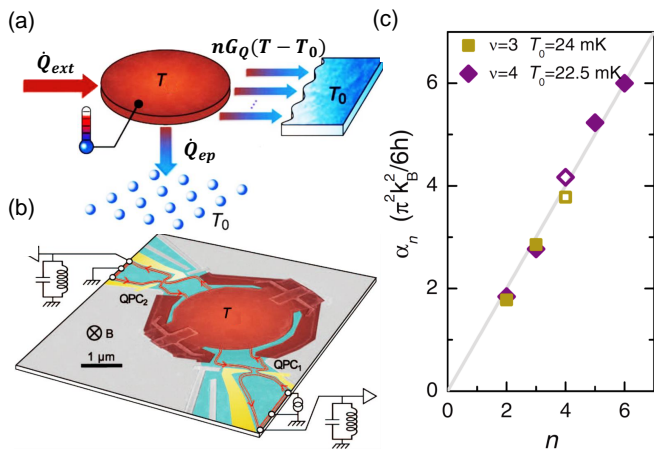


FIG. 8 Measuring quantized heat carried by electrons. (a) Applying Joule power \dot{Q}_{ext} to a metal plate (brown disk), the electronic temperature increases up to T and then the heat flows via n ballistic quantum channels to reservoir and to the phonon heat bath \dot{Q}_{ep} , which both have fixed temperature T_0 . (b) The colored scanning electron micrograph of the measured sample. In the center, the metallic ohmic contact in brown is connected to two quantum point contacts (QPC₁ and QPC₂) in yellow (lightest area) via a two-dimensional Ga(Al)As electron gas in light green (surrounding the point contacts). The red lines with arrows around the metal plate indicate the two propagating edge channels ($\nu = 3$ or $\nu = 4$). The Joule power is applied to the metallic plate through a QPC, and the two LC-tank circuits are for noise thermometry measurement. (c) The grey line shows the predictions for quantum limit of heat flow while the symbols exhibit the extracted electronic heat current normalized by $\pi^2 k_B^2 / 6h$ as a function of number of electronic channels n . Adapted from (Jezouin *et al.*, 2013).

Wharam *et al.*, 1988), Jezouin *et al.* (Jezouin *et al.*, 2013) measured the quantum-limited heat conductance of electrons in a quantum point contact. The principle and practical implementation of this experiment and its setup are shown in Fig. 8(a) and 8(b). A micrometer-sized metal plate is connected to both cold phonon bath and to a big electronic reservoir via an adjustable number n of ballistic quantum channels with both reservoirs at T_0 as shown in Fig. 8(a). By injecting Joule power \dot{Q}_{ext} to the metallic plate, the electrons were heated up to temperature T which can be directly measured by a noise thermometer. This power is then transmitted via the n quantum channels at the rate $nG_Q(T - T_0)$ through two quantum point contacts (QPC₁ and QPC₂) and to the phonon bath at rate \dot{Q}_{ep} which is independent of n . Both QPCs display clear plateaus of the measured electrical conductance at $n_1 e^2/h$ and $n_2 e^2/h$, respectively, where n_1 and n_2 are integers. The sum $n = n_1 + n_2$ determines the number of quanta carrying the heat out of the plate electronically. The structure used in this experiment (Jezouin *et al.*, 2013) satisfies the conditions of having sufficient electrical and thermal contact between the metal plate and the two-dimensional electron gas underneath.

Moreover the thermal coupling to the phonon bath and via the QPCs is weak enough such that the central electronic system forms a uniform Fermi gas (fast electron-electron relaxation and diffusion across the plate) at temperature T . A perpendicular magnetic field was applied to the sample for it to be in the integer quantum Hall effect regime at filling factors $\nu = 3$ or $\nu = 4$. Figure 8(c) shows α_n , the measured electronic heat conductance normalized by $\pi^2 k_B^2 / 6h$ as a function of the number n of electronic channels as symbols which fall on a straight line with unit slope shown by the grey line, thus demonstrating the quantized thermal conductance at the expected level. Equivalently this experiment demonstrates Wiedemann-Franz law on the current plateaus.

The work of (Jezouin *et al.*, 2013) was preceded already by two experiments, some two decades earlier (Chiatti *et al.*, 2006; Molenkamp *et al.*, 1992), where G_Q was tested with an order of magnitude accuracy. Both these measurements were performed on GaAs-based 2DEGs, and in both of them, thermal conductance was obtained by measuring the Seebeck coefficient (thermopower) and extracting the corresponding temperature difference. In (Molenkamp *et al.*, 1992), they then determined G_{th} which is within a factor two agreement with the assumption that Wiedemann-Franz law applies on their conduction plateaus of the QPC. In (Chiatti *et al.*, 2006), they made a similar experiment with the same philosophy but with improved control of the structure and system parameters. With these assumptions they come to a good agreement between thermal conductance and electrical conductance via the Wiedemann-Franz law.

In recent years, it has become possible to measure quantized thermal conductance even at room temperature (Cui *et al.*, 2017; Mosso *et al.*, 2017). The experiments are performed on metallic contacts of atomic size with scanning thermal microscopy probes. The material of choice is typically Au, although experiments on Pt have also been reported (Cui *et al.*, 2017). The setup and experimental observations of (Cui *et al.*, 2017) are presented in Fig. 9. The electrical conductance plateaus at multiples of $2e^2/h$ are typically seen when pulling the contact to the few conductance channel limit. The remarkable feature in the data is that the simultaneous thermometric measurement confirms the Wiedemann-Franz law for electric transport within 5 - 10% accuracy, thereby demonstrating quantized thermal conductance (Cui *et al.*, 2017).

In the measurement performed by (Banerjee *et al.*, 2017), the value of the quantum of thermal conductance for different Hall states including integer and fractional states was verified. First, they confirmed the observations of (Jezouin *et al.*, 2013) in a similar setup in the integer states with filling factors $\nu = 1$ and 2. Figure 10(a) demonstrates the validity of quantized heat conductance at $\Delta N G_Q$ for $\Delta N = 1, 2, \dots, 6$ channels with about 3% accuracy (inset). The main result of

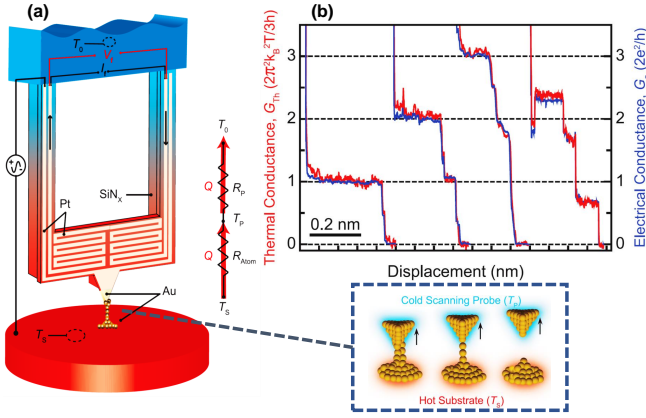


FIG. 9 Experimental setup and results on quantized thermal conductance in single atom junctions. (a) A calorimetric scanning thermal microscopy probe, which shows schematically how to make atomic junctions connected to a heated metallic substrate. By applying a small voltage bias and measuring the resulting current, the electrical conductance of the tip-substrate junction can be measured. T_S and T_0 are the temperatures of the substrate and the thermal reservoir, respectively. The zoom-out describes schematically the atomic chains forming, narrowing, and breaking during the withdrawal of the probe from the heated substrate. (b) The almost overlapping measured thermal (red, left) and electrical (blue, right) conductance traces normalized by $2\pi^2 k_B^2 T/3h$ and $2e^2/h$, respectively. Adapted from (Cui *et al.*, 2017).

the work is the observation of thermal conductance of strongly interacting fractional states. Figure 10(b) shows that the thermal conductance is again a multiple of G_Q even for the (particle-like) $\nu = 1/3$ fractional state, although the electrical conductance is normalized by the effective charge $e^* = e/3$. As a whole, the work covers both particle- and hole-like fractional states, testing the predictions of (Kane and Fisher, 1997).

As a final point for this Section we want to mention that there is a large number of further beautiful experiments on various heat transport effects performed in the quantum Hall regime. Not going into details of them here, we list a few of them for further reading: (Altimiras *et al.*, 2010; Banerjee *et al.*, 2018; Granger *et al.*, 2009; Halbertal *et al.*, 2016, 2017; Nam *et al.*, 2013; Sivre *et al.*, 2018; le Sueur *et al.*, 2010).

VII. PHOTONS

In this section we discuss transport by thermal microwave photons, presenting another important bosonic system to study in this context.

A. A ballistic photon channel

The concept of microwave photon heat transport becomes concrete when describing it on a circuit

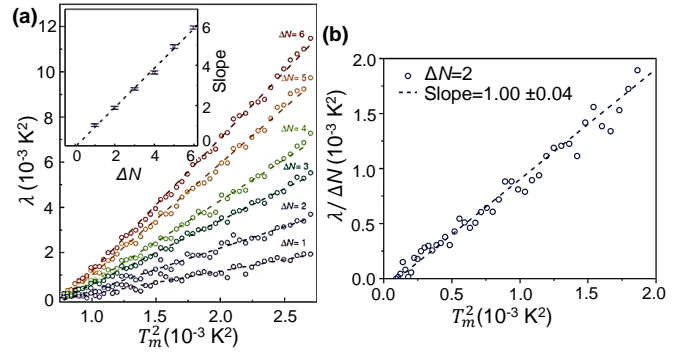


FIG. 10 Measurements in the integer (a) and fractional (b) quantum Hall regimes with filling factors $\nu = 2$ and $\nu = 1/3$, respectively. (a) The normalized coefficient of the dissipated power $\lambda = \delta P / (G_Q / 2T)$ as a function of T_m^2 for different configurations of $\Delta N = N_i - N_j$, where N is the number of channels. The difference is presented in order to eliminate the N -independent contribution of the phononic heat current. Here, δP is the difference between dissipated power at different N , $\delta P = \Delta P(N_i, T_m) - \Delta P(N_j, T_m)$, and T_m is the calculated temperature of the floating contact. The circles are showing the measured data and the dashed lines are linear fits to them. The slope of each set is shown in the inset as a function of ΔN . The linear dependence has approximately unit slope (0.98 ± 0.03) confirming the quantum of thermal conductance for this integer state $\nu = 2$. (b) The case of fractional state $\nu = 1/3$. Same as (a) but here the difference of λ between $N = 4$ and $N = 2$ normalized by ΔN as a function of T_m^2 . The slope of the linear fit (dashed line) to the measured data (circles) is very close to unity. Adapted from (Banerjee *et al.*, 2017).

level (Schmidt *et al.*, 2004). We start from a setup familiar from the century-old discussion by Johnson and Nyquist (Johnson, 1928; Nyquist, 1928). There two resistors R_1, R_2 are directly coupled to each other as shown in Fig. 11(a). They are generally at different temperatures T_1 and T_2 . Each resistor then produces thermal noise with the spectrum $S_v(\omega)$ of Eq. (32), i.e., they can be considered as photon sources. First we consider that R_1 generates noise current i_1 on resistor R_2 as $i_1 = v_1 / (R_1 + R_2)$. Then the spectral density of current noise is $S_{i_1}(\omega) = (R_1 + R_2)^{-2} S_{v_1}(\omega)$. The voltage noise produced by resistor R_i , $i = 1, 2$ is $S_{v_i}(\omega) = 2R_i \hbar \omega / (1 - e^{-\beta_i \hbar \omega})$, for $i = 1, 2$. The power density produced by noise of R_1 and dissipated in resistor R_2 is then $S_{P_2}(\omega) = \frac{R_2}{(R_1 + R_2)^2} S_{v_1}(\omega)$. The corresponding total power dissipated in resistor R_2 due to the noise of resistor R_1 is

$$\begin{aligned}
 P_2 &= \int_{-\infty}^{\infty} \frac{d\omega}{2\pi} S_{P_2}(\omega) \\
 &= \frac{4R_1 R_2}{(R_1 + R_2)^2} \int_0^{\infty} \frac{d\omega}{2\pi} \hbar \omega [n_1(\omega) + \frac{1}{2}], \quad (33)
 \end{aligned}$$

The net heat flux from 1 to 2, P_{net} , is the difference between P_2 and P_1 , where P_1 is the corresponding power produced by R_2 on R_1 by the uncorrelated voltage (cur-

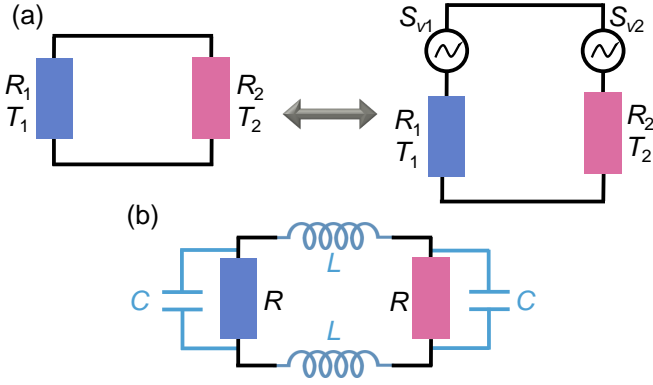


FIG. 11 The setup of two resistors R_1, R_2 at temperatures T_1, T_2 , respectively, interacting with each other via the respective thermal noises. We present the quantum version of the classical Johnson-Nyquist problem in the text with the associated radiative heat current. (a) The plain two-resistor heat exchange can be modeled by circuit approach where each resistor is accompanied with a thermal voltage noise source. The two sources are uncorrelated. (b) A realistic circuit includes inevitably reactive elements as well, as discussed in the text. These are added in the figure to allow for the analysis of the crossover between quantum and classical regimes upon varying the operating temperature and the physical system size.

rent) noise described similarly. Thus

$$P_{\text{net}} = \frac{4R_1R_2}{(R_1 + R_2)^2} \frac{\pi k_B^2}{12\hbar} (T_1^2 - T_2^2). \quad (34)$$

Note that the integrals for P_1 and P_2 separately (see Eq. (33)) would lead to a divergence due to the zero point fluctuation term, but since these fluctuations cannot transport energy, this term cancels out in the physical net power Eq. (34). We find that for a small temperature difference with $T_1 = T_2 \equiv T$

$$G_\nu = \frac{dP_{\text{net}}}{dT_1} \Big|_T = \frac{4R_1R_2}{(R_1 + R_2)^2} \frac{\pi k_B^2}{6\hbar} T, \quad (35)$$

which is equal to the quantum of heat conductance

$$G_\nu = G_Q \quad (36)$$

for $R_1 = R_2$. For a general combination of resistance values the factor

$$r = \frac{4R_1R_2}{(R_1 + R_2)^2} \quad (37)$$

represents a transmission coefficient. The circuit model for heat transport can be generalized to essentially any linear circuit composed of reactive elements and resistors as has been done, e.g., in (Pascal *et al.*, 2011; Thomas *et al.*, 2019).

B. Circuit limitations of the ballistic picture

What are the physical conditions for the experiment in a circuit to yield thermal conductance that is governed

by G_Q ? Certainly Johnson-Nyquist work (Johnson, 1928; Nyquist, 1928) was out of this domain, as well as an elegant more recent experiment by Ciliberto (Ciliberto *et al.*, 2013). The necessary key ingredients for "quantumness" are that the experiment combines low temperatures and physically small structures. More quantitatively, the realistic circuit is never presented fully by the simple combination of two resistors, but, instead the full picture of it includes also inevitable reactive elements. A way of describing a more realistic circuit (Golubev and Pekola, 2015) is to include a parallel capacitance and series inductance in the basic circuit, as shown in Fig. 11(b). The point is that electromagnetics tells us that an order of magnitude estimate for capacitance is given by $C \sim \epsilon \ell$ and inductance by $L \sim \mu_0 \ell$, where ℓ is the overall linear dimension of the circuit and ϵ and μ_0 are the permittivity and permeability of the medium. In order to observe the pure quantum thermal conductance, one needs to have a ballistic channel between the resistor baths, which in the present case means that the series inductor presents a small impedance and the parallel capacitance a large impedance. These both are to be compared to the resistances in the circuit, at all relevant frequencies meaning up to $\omega_{\text{th}} = k_B T / \hbar$, the thermal cut-off of the resistor at temperature T . In form of simple inequalities we then need to require $\omega_{\text{th}} L \ll R \ll (\omega_{\text{th}} C)^{-1}$, and based on our arguments above this transforms into

$$\epsilon \ell k_B T R / \hbar \ll 1, \text{ and } \mu_0 \ell k_B T / (\hbar R) \ll 1. \quad (38)$$

It is now easy to verify the statements in the beginning of this subsection. We assume for simplicity a typical value for a resistance used in some experiments, $R = 100 \Omega$. If we take a mesoscopic circuit with $\ell = 100 \mu\text{m}$ at a low temperature, $T = 100 \text{ mK}$, we find that $\epsilon \ell k_B T R / \hbar \approx \mu_0 \ell k_B T / (\hbar R) \approx 0.01$ satisfying the conditions in Eqs. (38). On the other hand a $\ell = 0.1 \text{ m}$ macroscopic circuit at room temperature $T = 300 \text{ K}$ yields $\epsilon \ell k_B T R / \hbar \approx \mu_0 \ell k_B T / (\hbar R) \approx 3 \times 10^4$, far in the classical regime. Some of those conditions can be avoided in a low temperature transmission line circuit (Partanen *et al.*, 2016) as will be discussed below.

C. Experiments on heat mediated by microwave photons

We modelled in Section VII the heat emitted by a resistor and absorbed by another one in an otherwise dissipationless circuit. It was shown (Schmidt *et al.*, 2004) that this heat carried by microwave photons behaves as if the two resistors were coupled by a contact whose ballisticity is controlled by the impedances in the circuit. Ideally two physically small and identical resistors at low temperatures can come very close to the ballistic limit with thermal conductance approaching G_Q . Motivated by this observation, several experiments assessing this result were set up during the past two decades (Meschke

et al., 2006; Partanen *et al.*, 2016; Timofeev *et al.*, 2009). They were all performed essentially in the same scenario: the resistors are normal metallic thin film strips with sufficiently small size such that their temperature varies significantly in response to typical changes of power affecting them. The electrical connection between the resistors is provided by superconducting (aluminum) leads, whose electronic heat conductance is vanishingly small at the temperature of operation, see Section IV.A. In one of the experiments ((Meschke *et al.*, 2006)) the superconducting lines are interrupted by a SQUID that acts as a tunable inductor providing a magnetic flux controlled valve of photon mediated heat current. All these experiments are performed at $T \sim 0.1$ K, far below $T_C \approx 1.4$ K of aluminum. Temperatures are controlled and monitored by biased NIS tunnel junctions.

The experiment of Timofeev *et al.* (Timofeev *et al.*, 2009) was designed to mimic as closely as possible the basic configuration of Fig. 11(a) with a superconducting (Al) loop. In this case the distance between the resistors was about $50 \mu\text{m}$ and the temperatures of both the heated (or cooled) source and the drain resistor were measured. The experiment (Fig.12(a-c)) demonstrates thermal transport via the electronic channel, i.e. quasiparticle thermal transport (Bardeen *et al.*, 1959) described in Section IV.A, at temperatures exceeding ~ 250 mK. The result in this regime is well in line with the basic theory, taken the dimensions and material parameters of the aluminum leads. More importantly, below about 200 mK the photon contribution kicks in. In the loop geometry it turns out that the temperatures of the two resistors follow each other closely at lowest bath temperatures, yielding thermal conductance given by G_Q . Some uncertainty remains about the absolute value of G_ν since the precise magnitude of the competing electron-phonon heat transport coefficient Σ remained somewhat uncertain. The measurement was backed by a reference experiment, where a similar sample as that described above was measured under the same conditions and fabricated in the same way. This reference sample lacked intentionally one arm of the loop leading to poor matching of the circuit in the spirit discussed in Section VII.B. In this case the quasiparticle heat transport prevails as in the matched sample, but the photon G_ν is vanishingly small, confirming, one could say even quantitatively, the ideas presented about the heat transfer via a non-vanishing (reactive) impedance.

The experiment described above was performed on a structure with physical dimensions not exceeding $100 \mu\text{m}$. A natural question arises: is it possible to transport heat over macroscopic distances by microwave photons, like radiating the heat away from the whole chip? This could be important for example in quantum information applications (for superconducting qubit realizations, see (Kjaergaard *et al.*, 2020)). This question was addressed experimentally by (Partanen *et al.*, 2016)

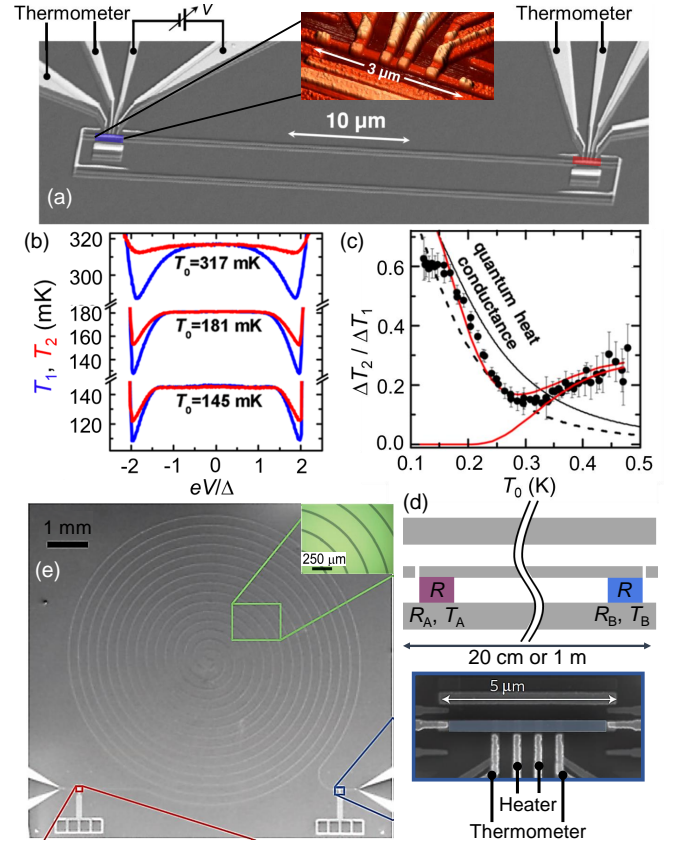


FIG. 12 Quantum-limited heat conduction over microscopic and macroscopic distances. (a) The scanning electron micrograph (SEM) of two AuPd resistors at a distance of $50 \mu\text{m}$ are connected via Al superconducting lines into a loop to match the impedance between them to reach the full quantum of heat conductance. NIS probe junctions are used to apply Joule heat and to measure the island temperature. (b) Measured local island temperature, T_1 (blue) and remote one T_2 (red) as functions of applied bias voltage on cooler/heater NIS junction pairs at different bath temperatures T_0 . The drop for T_1 is naturally stronger than that for T_2 . (c) The measured relative temperature drops (symbols) $\Delta T_2/\Delta T_1$ against T_0 at the optimum cooling bias voltage obtained from data like those in (b). The descending solid and dashed black lines are obtained from the linearized thermal model, which is simply given by $\Delta T_2/\Delta T_1 = G_x/(G_x + G_{\text{th},2})$ (see Fig. 2(b)) at low temperatures. The thermal model is that shown in Fig. 2(b). The electron-phonon constant considered to be $\Sigma_{\text{AuPd}} = 2 \times 10^9 \text{ WK}^{-5} \text{ m}^{-3}$ and $\Sigma_{\text{AuPd}} = 4 \times 10^9 \text{ WK}^{-5} \text{ m}^{-3}$ for the solid and dashed lines, respectively. The remaining red solid lines are the results of the numerical thermal model. (d) A superconducting transmission line terminated at the two ends by normal-metal resistances R_A and R_B at two different electron temperatures T_A and T_B , respectively, is schematically shown. (e) SEM image of an actual device, where the length of the coplanar waveguide (transmission line), made out of Al, is either 20 cm or 1 m and has a double-spiral structure. The SEM image of the zoom-out of one of the resistors (made out of either AuPd or Cu) with a simplified measurement scheme is shown in the bottom right of the figure. (a-c) Adapted from (Timofeev *et al.*, 2009) and (d-e) adapted from (Partanen *et al.*, 2016).

(Fig.12(d-e)), who placed the two resistors at a distance of about 10 mm, i.e. about 100 times further away from each other as compared to what was done earlier. Furthermore, the connecting line between the two baths was a 1 m long meander made of a superconductor, acting as a transmission line. Such a coplanar line has typically an impedance of about 50Ω irrespective of its length, thus potentially supporting the heat transport even over large distances. The thermal conductance was measured as in Timofeev *et al.* (Timofeev *et al.*, 2009), with similar results proving the hypothesis of photon transport over macroscopic distances. These experiments may open the way for practical heat transport schemes in microwave circuits.

VIII. TUNABLE QUANTUM HEAT TRANSPORT

In this section we describe quantum systems where heat transport is controlled by either magnetic or electric field to achieve useful functional operation. These devices include heat valves, heat interferometers, thermal rectifiers and circuit refrigerators. Mesoscopic structures provide an option to control currents by external fields. Concerning charge currents, SQUIDS (Tinkham, 2004) and single-electron transistors (Averin and Likharev, 1991) provide hallmark devices in this context, where magnetic field (flux in a superconducting loop) and electric field (gate voltage), respectively, are the parameters that control the current.

The first experiment on heat transport by thermal microwave photons (Meschke *et al.*, 2006) was realized in a setup where a SQUID is used as a heat valve. The experiment depicted in Fig. 13 shows two metallic (AuPd) resistors at the distance of few tens of μm from each other, connected by superconducting (Al) lines. The loop is interrupted in each arm by a SQUID, whose flux can be controlled by the common external field for both of them. The thermal model of Fig. 2(b) applies to this circuit. In the experiment only the heated resistor's temperature T_{e1} was measured. The panel at bottom right displays the magnetic flux dependent variation of temperature T_{e1} at different bath temperatures T_0 under a constant level of heating. At bath temperatures well above 100 mK, the flux dependence vanishes, since the inter-resistance thermal conductance by photons, $\propto T$, is much weaker than the conductance to the phonon bath, $\propto T^4$. On the contrary, towards low temperatures below 100 mK, the electron temperature T_{e1} varies with magnetic flux as the inter-resistor coupling becomes comparable to the bath-coupling, demonstrating the photonic thermal conductance. Moreover, the magnitude of the thermal conductance was shown to follow from the circuit model presented in Section III.A quantitatively, when applied to the current setup. Among other things, the data and this calculation predicted that at $T_0 = 60$ mK the maxi-

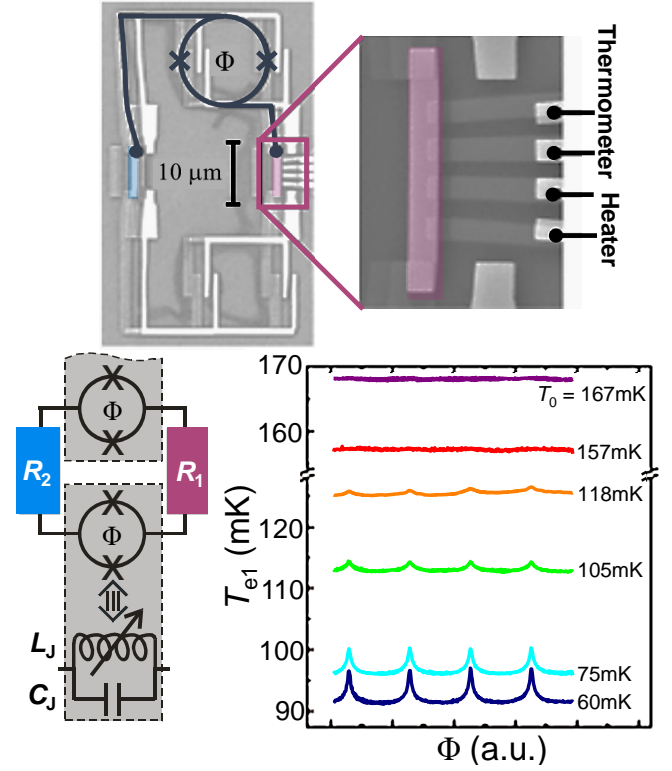


FIG. 13 Photon thermal transport controlled by magnetic flux. (top left) The SEM of the device, where two nominally identical normal-metal resistors R_1 and R_2 (colored in blue and red on the left and right, respectively), made out of AuPd, are connected to each other via two aluminum superconducting leads, interrupted by a DC-SQUID (a superconducting loop with two Josephson junctions shown by the cross sign) in each line. The SQUIDS again serve as thermal switches between the resistors and can be controlled by external magnetic flux Φ . (top right) Magnified view of R_1 , connected to four NIS tunnel junctions to the right and to two NS contacts at top and bottom to allow thermometry and Joule heating. (bottom left) Schematic illustration of the electrical model of the actual sample. (bottom right) Measured flux modulation of the electron temperature T_{e1} in R_1 as a function of applied magnetic flux Φ for different values of bath temperature T_0 . The modulation decreases monotonically by increasing T_0 because of stronger coupling to the phonon bath. The maxima in T_{e1} correspond to the weakest electron-photon coupling at half-integer values of Φ/Φ_0 where $\Phi_0 = h/2e$ is the magnetic flux quantum. Adapted from (Meschke *et al.*, 2006).

imum value of thermal conductance with zero flux in the SQUID (i.e. with minimum Josephson inductance) was $\sim 50\%$ of G_Q .

Photonic heat current was controlled by magnetic field in the previous example. A dual method is to apply electric field as a control as indicated in Fig. 14(a). This procedure was realized in the experiment recently (Maillet *et al.*, 2020), where the superconducting loop is interrupted by a Cooper-pair transistor ("charge qubit" (Nakamura *et al.*, 1999)). In this setup, the Josephson coupling is tuned by the gate voltage. The

thermal model of the experiment is pretty much as before, only the Josephson element with its control field is different. Electric field by gate voltage is in general easier to apply, especially locally on the chip, as compared to local magnetic flux. As shown by Fig. 14(a), the device demonstrated gate-dependent modulation of heat current. Its overall magnitude is consistent with the modeling of the circuit: at maximum thermal conductance $G_\nu \approx 0.35G_Q$ was achieved.

As to the heat currents in single-electron circuits, similar control principles apply, in general. An early experiment to control heat flow by a gate voltage in a single-electron transistor formed of NIS junctions was performed by (Saira *et al.*, 2007). The results on temperature of the system were confirmed quantitatively by a model employing standard single-electron tunneling theory and heat balance equation on the measured central island of the transistor. Heat transport via a fully normal metallic single-electron transistor was measured by (Dutta *et al.*, 2017). Results of this experiment are shown in Fig. 14(b). The heat current between the source and drain with a temperature bias applied across was carried by electrons and modulated by the gate voltage such that the observed thermal conductance and simultaneously measured electrical conductance go hand in hand. Yet, deviations from the Wiedemann-Franz law due to Coulomb blockade and quantum tunneling were observed in agreement with the theory (Kubala *et al.*, 2008). Recently, deviations from Wiedemann-Franz law were observed in a similar setup with a semiconducting InAs quantum dot transistor (Majidi *et al.*, 2021).

A. Electronic quantum heat interferometer

Another quantum interference experiment on heat current by electrons was performed by (Giazotto and Martínez-Pérez, 2012), shown in Fig. 15. They used a magnetic field controlled SQUID as an interferometer. They could independently measure the electrical and heat transport via the device. For the latter, the SQUID was placed between two mesoscopic heat baths and the heat current was measured with the principle that was depicted in Fig. 2(b). The measurement was performed in a temperature regime exceeding that described in Section IV.A such that T is high enough for the superconductor to have a substantial equilibrium quasiparticle population (i.e. not all electrons are paired). In this regime the superconductor as such can support heat current, and heat interference across the Josephson junctions of the SQUID becomes possible. This work addressed experimentally for the first time a half-a-century old proposal and theory (Maki and Griffin, 1965) which has been followed by several works more recently (Golubev *et al.*, 2013; Guttman *et al.*, 1998, 1997; Zhao *et al.*, 2003). It also demonstrated potential of electronic caloritronics in

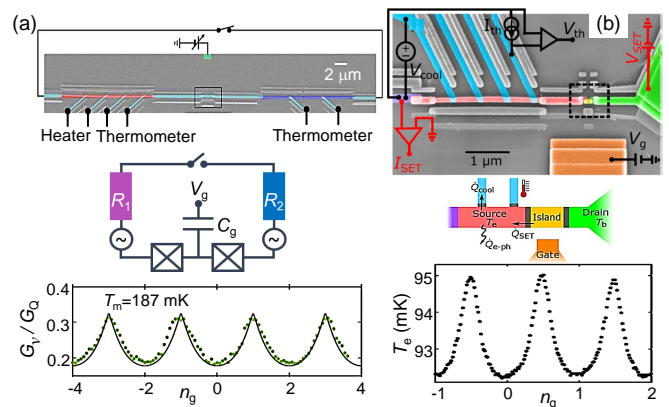


FIG. 14 (a) The SEM (top) and the equivalent electrical circuit diagram (middle) of the device including a Cooper-pair transistor coupled to two normal-metal resistors R_1 and R_2 at temperatures T_1 and T_2 , respectively. (bottom) Measured thermal conductance (symbols) normalized by G_Q as a function of gate charge $n_g = C_g V_g / e$ at $T_m = (T_1 + T_2)/2$. The solid line indicates the theoretical expectation. (b) The SEM image (top) and the schematic realization (middle) of the device consisting of a single-electron transistor and the heat transport measurement setup. The black circuit on the top left corner displays the heat transport setup. (bottom) Measured gate dependence of the electronic temperature T_e of the source island when it is lower than the bath temperature T_0 . (a) Adapted from (Maillet *et al.*, 2020) and (b) adapted from (Dutta *et al.*, 2017).

superconducting circuits.

B. Cooling a quantum circuit

In the experiment performed by (Tan *et al.*, 2017) photon-assisted tunneling serves the purpose of decreasing the number of microwave quanta in a superconducting quantum circuit, namely a coplanar wave resonator (harmonic oscillator). The optical micrograph of the sample presented in Fig. 16(a) shows resistive elements inserted at the two ends of the resonator, acting as heat sinks for it. Figure 16(b) displays the temperature of one of these resistors (Quantum Circuit Refrigerator, QCR), measured and controlled by NIS tunneling, effectively lowering and elevating the electronic temperature of it depending on the biasing of the cooler junction, see Section IV.B. The other resistor (“Probe”) is passive but its temperature is likewise monitored. This temperature reacts weakly to the QCR temperature changes. The authors in (Tan *et al.*, 2017) develop a thermal model based on which they extract the average number of photons in the resonator and the corresponding temperature T_{res} . In this experiment $T_{\text{res}} \approx 800$ mK far exceeds all other temperatures, most notably the electronic temperatures of the two resistors, $T_{\text{QCR}} \approx T_{\text{probe}} \approx 150$ mK even under no bias on the QCR. The model then predicts cooling of the resonator down to about 400 mK under optimal

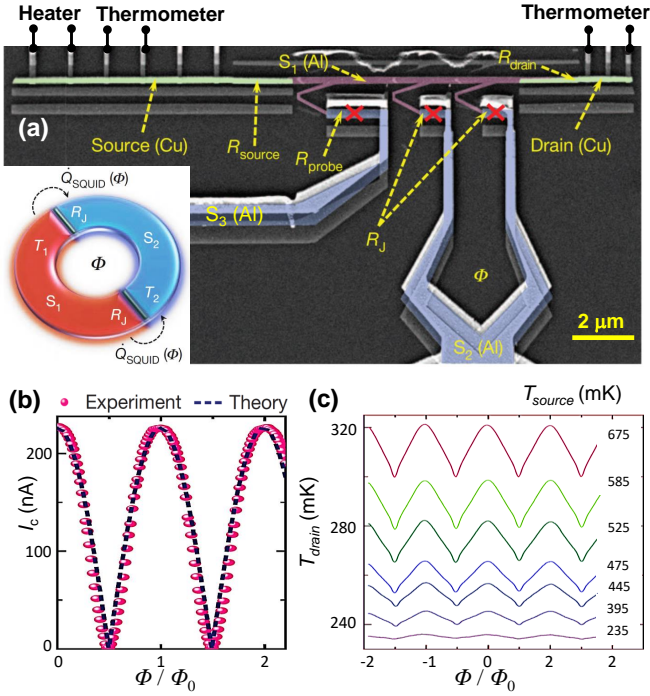


FIG. 15 Josephson heat interferometer. (a) The SEM of the device. The source and drain electrodes made out of Cu are connected to an Al island (S_1) through two AlO_x tunnel barriers. S_1 is connected sideways to a DC-SQUID which is terminated to a large-volume lead S_2 (Al) for thermalization and to an Al tunnel probe (S_3) for independent SQUID characterization. NIS junctions in source and drain are used to heat and monitor the temperature of each island. Red crosses indicate the Josephson junctions. The core of the device (SQUID) is shown schematically in the inset. Two identical superconductors with different temperatures are connected with the two tunnel junctions of the SQUID. Applying magnetic flux Φ the heat current $\dot{Q}_{\text{SQUID}}(\Phi)$ from hot to cold is varying. (b) Maximal charge current of the SQUID I_c as a function of Φ at 240 mK bath temperature. The dashed line presents the theoretical result assuming 0.3% asymmetry in the junctions, and symbols are experimental data. (c) Flux modulation of T_{drain} related to heat current measured at different T_{source} values. Here the bath temperature is fixed at 235 mK. Adapted from (Giazotto and Martínez-Pérez, 2012).

biasing conditions of the QCR (Fig. 16(c)). Based on the parameters given in the manuscript, one would estimate the resonator to have $T_{\text{res}} \approx 200$ mK when the QCR is not biased. Indeed, in a later work (Masuda *et al.*, 2018) resonator temperatures in the 200 mK regime were reported at zero bias. When biased, the NIS junctions operate as an incoherent microwave source. Then the mode temperature of the resonator can be driven even beyond 2.5 K, far above the temperature of the phonon and electron reservoirs of the system (Masuda *et al.*, 2018). This phenomenon was theoretically modelled by (Silveri *et al.*, 2017) using photon-assisted tunneling of the biased, NIS-junctions as the environment. The effective temperature of the resonator is expected to be lifted to $\sim eV/(2k_B)$

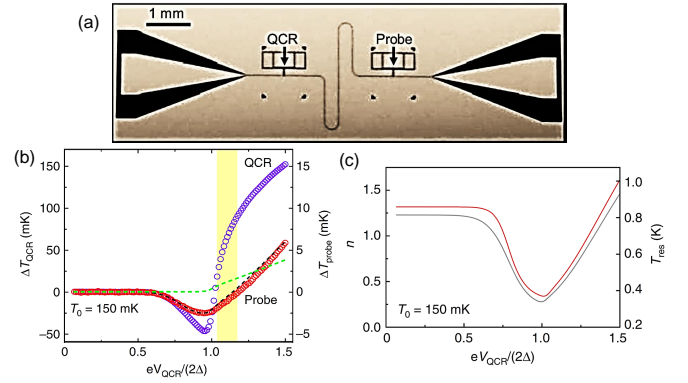


FIG. 16 Quantum circuit refrigerator (QCR). (a) Optical micrograph of a sample, where a superconducting coplanar-waveguide resonator is in the center coupled to a QCR and a probe resistor indicated by the arrows. (b) Measured changes in the electron temperature of QCR, ΔT_{QCR} with purple circles, and the probe resistor, ΔT_{probe} , with red circles, as functions of the refrigerator operation voltage V_{QCR} . The black dashed line, following the probe data closely, and green dashed line show the given theoretical results on ΔT_{probe} , including and excluding photon-assisted tunneling, respectively. (c) Average number of photons n and the corresponding effective temperature of the resonator T_{res} shown with the two solid lines in red and grey, based on the thermal model introduced in (Tan *et al.*, 2017). Adapted from (Tan *et al.*, 2017).

at bias voltage V .

IX. QUANTUM HEAT TRANSPORT MEDIATED BY A SUPERCONDUCTING QUBIT

In this section we introduce a superconducting qubit as an element that mediates heat by microwave photons between two baths. Different types of superconducting quantum bits, e.g. flux, charge and transmon qubits to mention a few common ones, are options in such devices (Clarke and Wilhelm, 2008). They feature different coupling options and strengths, as well as different degrees of anharmonicity in the Josephson potential to be discussed below. In the experiments of (Ronzani *et al.*, 2018) transmon type qubits (Koch *et al.*, 2007) were employed. This kind of a qubit has levels whose positions can be controlled by magnetic flux through the SQUID-loop. Transmon qubit is only weakly anharmonic, meaning that one typically needs to consider not only the two lowest levels (that form the actual qubit) but also the higher levels in this nearly harmonic potential. One should point out an important difference: although even weak anharmonicity is enough to address only the two lowest levels in a microwave-driven experiment, one needs, on the contrary, to consider higher levels as well, when the qubit sees a thermal bath with wide spectrum. Yet in a typical experiment to be described here, the separation of the levels is of the order of 0.5 K, meaning

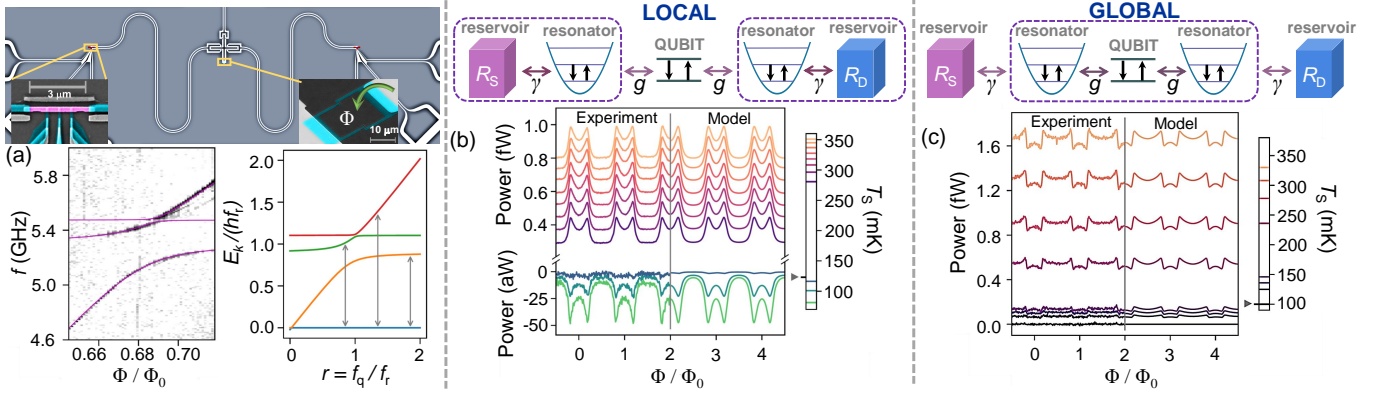


FIG. 17 Quantum heat valve: the local and global regimes. (a) The top panel shows the quantum heat valve device where transmon-type superconducting qubit in the center is capacitively coupled to two similar $\lambda/4$ coplanar waveguide resonators made out of Nb. Each resonator is terminated by a normal-metal resistor (Cu) acting as a reservoir. The insets display the SEM images of the SQUID which can be controlled by magnetic flux Φ , and one of the two reservoirs (pink, in the center) whose temperature is monitored and controlled by NIS probes (Cu-AlO_x-Al). The lower panels show the two-tone transmission spectroscopy (left) and the corresponding theoretical positions (right) for the structure shown on top without resistors. (b,c) The top panels show the schematic illustrations of the two regimes. The resulting heat transport data are shown in the lower panels, where the flux dependence of the heat current in the drain reservoir in the two regimes is measured. Each trace corresponds to a different temperature T_S of the source reservoir shown in the legend bar. Adapted from (Ronzani *et al.*, 2018).

that the thermal population of the third level is already quite small at the low temperatures of the experiment, say, below 0.2 K ($\sim e^{-5} < 0.01$).

In this Section we present thermal transport experiments under the conditions where the qubit is not driven. Coherent properties of the qubit do not then play any important role. In the future the same devices will be driven by RF-fields and evolution of off-diagonal elements of the density matrix will develop as well.

A. Quantum heat valve

Figure 17(a) shows on the top a typical experimental configuration of heat control with qubit, taken from (Ronzani *et al.*, 2018). The energy separation of the transmon qubit (center) can be controlled by external magnetic flux Φ . The qubit is coupled capacitively (coupling g) to two nominally identical superconducting coplanar wave resonators that act as LC resonators with a resonant frequency of ~ 5 GHz each. For thermal transport experiments the $\lambda/4$ resonators are terminated by on-chip resistors which form the controlled dissipative elements in the circuit (Chang *et al.*, 2019). The dissipation is then given by the inverse of the quality factor of the resonator and can be quantified by another coupling parameter γ . In this circuit, which is called a quantum heat valve, heat is carried wirelessly (via capacitors) by thermal microwave photons over a distance of few millimeters from one bath to another. A schematic model of such a coupled circuit is shown in panels 17(b) and 17(c) on top.

It turns out that the measurement of heat transport

in such a circuit addresses some fundamental questions of open quantum systems (Aurell and Montana, 2019; Chiara *et al.*, 2018; Donvil *et al.*, 2020, 2018; Hewgill *et al.*, 2020; Hofer *et al.*, 2017; Levy and Kosloff, 2014; Magazzù and Grifoni, 2019; Rivas *et al.*, 2010). There are (at least) two possible ways of viewing the circuit, namely the local view (Fig. 17(b)) and the global view (Fig. 17(c)). In the local picture as we define it, the environment of the qubit is formed of the dissipative LC resonator with Lorentzian noise spectrum centered around its resonance frequency. In this regime, which occurs when $\gamma \gg g$, the system acts indeed as a valve admitting heat current through only when the qubit frequency matches (within the range determined by the quality factor) the frequency of the resonators. This results in Lorentzian peaks in power centered at flux positions corresponding to the said matching condition, demonstrated by both experiment and theory, shown in the bottom panel of Fig. 17(b). In the opposite limit, in the global regime, when $\gamma \ll g$, the situation is different. The combined system composed of the resonators and the qubit then make up a hybrid that interacts with bare environment formed of the two resistors. In this limit the hybrid quantum system has the energy spectrum shown in the bottom panel of Fig. 17(a) exhibiting multilevel structure. This is shown by the basic calculated spectrum and the spectroscopic measurement on a structure similar to that in the top panel but in the absence of the resistive loads. The data in Fig. 17(c) demonstrates results in the global regime, with experiment and theory developed in (Ronzani *et al.*, 2018) in agreement with each other. This experiment is the first one to assess

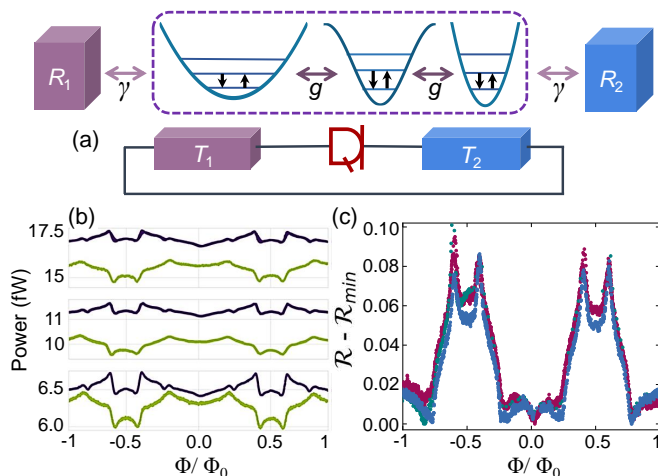


FIG. 18 Heat rectification using a transmon qubit (Senior *et al.*, 2020). (a) A schematic illustration of a photon diode composed of an anharmonic oscillator (qubit), coupled to two LC resonators with largely different resonance frequencies. The bottom panel in (a) shows a circuit view of the system, where we assign the quantum heat rectifier in the middle by the red symbol. (b) Dependence of source-drain heat current (power) as a function of magnetic flux in forward ($1 \rightarrow 2$, dark line, P^+) and reverse ($2 \rightarrow 1$, light line, P^-) directions under identical but opposite bias conditions at few different source temperatures (420, 400 and 380 mK from top to bottom). (c) Rectification ratio $\mathcal{R} = P^+/P^-$ (with its minimal value subtracted) as a function of magnetic flux for the data in (b) at the three temperatures of the source. Adapted from (Senior *et al.*, 2020).

local-global crossover in the spirit of locating the Heisenberg cut between the quantum and classical worlds. In a recent theoretical analysis, the authors of this review analyzed the cross-over behavior between the two limiting regimes with the help of direct solution of the Schrödinger equation including an oscillator bath (Pekola and Karimi, 2020).

B. Thermal rectifier

In a symmetric structure as in Fig. 17, there is naturally no directional dependence of heat transport between the two baths. However, heat current rectification becomes possible if one breaks the symmetry of the structure (Segal and Nitzan, 2005). Heat rectification (Bhandari *et al.*, 2021; Goury and Sánchez, 2019; Iorio *et al.*, 2021; Kargı *et al.*, 2019; Motz *et al.*, 2018; Riera-Campeny *et al.*, 2019; Ruokola *et al.*, 2009; Sánchez *et al.*, 2015; Segal and Nitzan, 2005; Sothmann *et al.*, 2012) can be quantified in different ways, but in general finite rectification means that the magnitudes of forward and reverse heat currents differ under identical but opposite temperature biasing conditions. There exist a few experiments on heat current rectification, e.g. on phonons in carbon nanotubes (Chang *et al.*, 2006), and electrons

in quantum dots (Scheibner *et al.*, 2008), mesoscopic tunnel junctions (Martínez-Pérez *et al.*, 2015) and suspended graphene (Wang *et al.*, 2017). In (Senior *et al.*, 2020) rectification was realized in a structure similar to that in Fig. 17 but by making the two resonators of unequal length: the two resonators had in this case frequencies 3 GHz and 7 GHz. An additional feature necessary for heat rectification is the non-linearity of the central element, which arises from the anharmonicity of the transmon Josephson potential. Figure 18 shows data from (Senior *et al.*, 2020) where heat current through the structure is measured in forward and reverse directions under the same but opposite temperature biasing, respectively. Complicated flux dependence can be observed, but the main feature is that one reaches 10% rectification at best and it depends strongly on the flux position determining the coupling asymmetry to the two baths. Quantitative analysis of the flux dependence is challenging and experiments in simpler setups would be welcome.

X. HEAT CURRENT NOISE

In this section we focus on fluctuations of currents, which are generally considered to be harmful, and something to get rid of. The synonym of fluctuations, noise, proposes this negative side of the concept of fluctuations. Noise typically determines the minimal detectable signal in a measurement, i.e. the resolution. Here we do not consider noise caused by the measurement apparatus or from other extrinsic sources, but we focus on intrinsic noise, due to fundamental quantum and thermal fluctuations. This noise, for instance in form of electrical current or heat current fluctuations determines the ultimate achievable measurement accuracy. But besides being a limiting factor of a measurement, noise can also serve as a signal to build on in order to realize a sensor: for instance, measurement of thermal current noise of a conductor provides one of the most popular and fundamental thermometers in use (Fleischmann *et al.*, 2020).

We already discussed current and voltage noise of a linear dissipative element in Section IV.D. Here we review the heat current noise, both classical and quantum, see e.g. (Crépieux, 2021; Karimi and Pekola, 2021; Moskalets, 2014; Pekola and Karimi, 2018; Sánchez and Büttiker, 2012). For simplicity, we consider first the tunneling as an example. Besides presenting the classical fluctuation-dissipation theorem for heat current, which we review in a general case after it, we also observe the intriguing quantum expression of heat current noise including the frequency dependent component due to zero point fluctuations surviving down to $T = 0$. Next we focus on the temperature dynamics of a finite system coupled to a bath, which yields the experimentally accessible fundamental fluctuations of the effective temperature of this subsystem. Finally we review the experimental situa-

tion, with up to now only a small number of examples, on fluctuations in heat transport of quantum and classical systems.

A. FDT for heat in tunneling

We consider tunneling where the average heat current out from lead L was given by Eq. (18). Taking for simplicity the normal conductors (NIN junction) with $n_L(\epsilon) = n_R(\epsilon) = 1$, we have the average heat current at $eV = 0$

$$\dot{Q}_L = \frac{1}{e^2 R_T} \int d\epsilon \epsilon [f_L(\epsilon) - f_R(\epsilon)]. \quad (39)$$

The thermal conductance for tunneling, $G_{\text{th}} = \frac{d\dot{Q}_L}{dT_L}|_{T_L=T}$, is then given by $G_{\text{th}} = \mathcal{L}TG_T$, where $G_T = 1/R_T$ is the conductance of the tunnel junction. Like the fully transmitting channels in Section II, the tunnel junction satisfies the Wiedemann-Franz law.

The heat current operator \hat{H}_L to obtain the average heat current of Eq. (18) was calculated using the tunnel coupling operator of Eq. (16) and commuting this with the Hamiltonian of the left lead. We may use this operator to find the two-time correlator of it and Fourier-transform to find the spectral density of noise of heat current at finite (angular) frequency ω (but at $eV = 0$) as $S_{\dot{Q}}(\omega) = \int dt \langle \hat{H}_L(t) \hat{H}_L(0) \rangle e^{i\omega t}$ yielding (Averin and Pekola, 2010; Karimi and Pekola, 2021; Sergi, 2011; Zhan *et al.*, 2013)

$$S_{\dot{Q}}(\omega) = \frac{G_T}{6e^2} [(2\pi k_B T)^2 + (\hbar\omega)^2] \frac{\hbar\omega}{1 - e^{-\hbar\omega/k_B T}}. \quad (40)$$

For the symmetrized noise, $S_{\dot{Q}}^{(s)}(\omega) = \frac{1}{2}[S_{\dot{Q}}(\omega) + S_{\dot{Q}}(-\omega)]$, we then have

$$S_{\dot{Q}}^{(s)}(\omega) = \frac{G_T}{12e^2} [(2\pi k_B T)^2 + (\hbar\omega)^2] \hbar\omega \coth\left(\frac{\hbar\omega}{2k_B T}\right). \quad (41)$$

Now there are two important limits to consider. First of all, for $\omega \rightarrow 0$, we obtain the classical fluctuation-dissipation theorem for heat current as

$$S_{\dot{Q}}^{(s)}(0) = 2k_B T^2 G_{\text{th}}. \quad (42)$$

On the other hand, the finite frequency noise does not vanish at zero temperature, but

$$S_{\dot{Q}}^{(s)}(\omega) = \frac{G_T}{12e^2} |\hbar\omega|^3, \quad T = 0. \quad (43)$$

B. FDT for heat for a general system

The previous sub-section serves as an illustration of how noise and dissipation are related. Here we extend

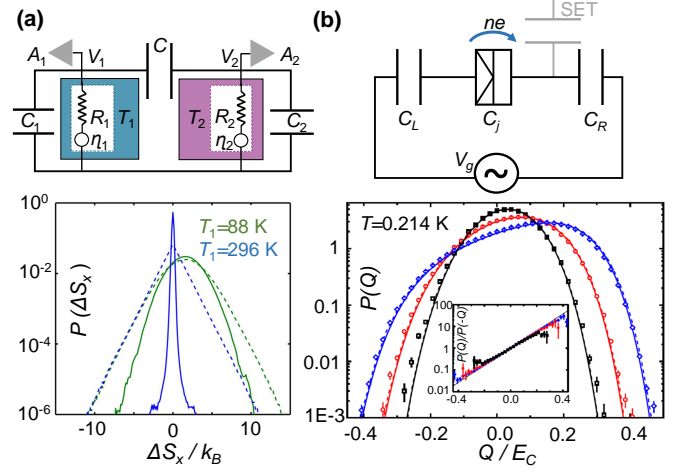


FIG. 19 Indirect measurements of noise of heat current and entropy production. (a) Upper panel shows the circuit diagram where two resistors R_1 and R_2 at temperatures T_1 and $T_2 = 296$ K, respectively, are coupled via the capacitance C . C_i , V_i , and A_i with $i = 1, 2$ show schematically the capacitance of the cables and input amplifiers, applied voltages, and low noise amplifiers, respectively. The probability of the entropy production due to the heat exchanged with the reservoirs $P(\Delta S_r)$ (dashed lines) and the probability of the total entropy $P(\Delta S_{\text{tot}})$ (solid lines) measured at different temperatures. Blue lines correspond to equilibrium where both distributions are centered symmetrically around zero and green lines are for out of equilibrium case with shifted distributions towards positive value. (b) In the upper panel, the electron box is formed by two metallic electrodes which are coupled by a tunnel junction with capacitance C_j , and connected capacitively to the voltage source via C_L and C_R . The box is also connected to a single electron transistor (SET) working as an electrometer shown by gray line. The lower panel shows the measured distribution of the generated heat $P(Q)$ at three different drive frequencies: 1 Hz (black squares), 2 Hz (red circles), and 4 Hz (blue diamonds). The solid lines are exact theoretical predictions and dashed lines show the results of Monte Carlo simulations. Inset: The solid line displays the Crooks fluctuation theorem and the symbols show $P(Q)/P(-Q)$ ratio for the experimental distributions. (a) Adapted from (Ciliberto *et al.*, 2013) and (b) adapted from (Saira *et al.*, 2012b).

the discussion to a general setup beyond the tunneling case. This would allow us to treat other mechanisms as well, for instance phonons, photons and electron-phonon coupling relevant for the current review. In general the FDT for heat applies in the form introduced in Eq. (42) for low frequency noise. To see this we may write the Hamiltonian

$$\mathcal{H} = \hat{H}_s + \hat{H}_b + \hat{H}_c \equiv \hat{H}_0 + \hat{H}_c, \quad (44)$$

where the unperturbed Hamiltonian $\hat{H}_0 = \hat{H}_s + \hat{H}_b$ is composed of the system and bath and \hat{H}_c is again the coupling. Then in linear response, we have the expecta-

tion value of the heat current to the system

$$\dot{Q} = \langle \dot{H}_s \rangle = -\frac{i}{\hbar} \int_{-\infty}^0 dt' \langle [\dot{H}_s(0), \hat{H}_c(t')] \rangle_0, \quad (45)$$

The expectation value of a general operator \mathcal{O} in the non-interacting system is written as $\langle \mathcal{O} \rangle_0 = \text{Tr}(e^{-\beta_s \hat{H}_s} e^{-\beta \hat{H}_b} \mathcal{O}) / \text{Tr}(e^{-\beta_s \hat{H}_s} e^{-\beta \hat{H}_b})$, where $\beta_s = 1/k_B T_s$ and $\beta = 1/k_B T$ are the corresponding inverse temperatures of the system and bath, respectively. By definition, the thermal conductance is given by

$$G_{\text{th}} = -\frac{d\dot{Q}}{dT_s} \Big|_{T_s=T} = \frac{1}{k_B T^2} \langle \delta \hat{H}_s \dot{H}_s \rangle_0, \quad (46)$$

where we used $\hat{H}_s - \langle \hat{H}_s \rangle_0 \equiv \delta \hat{H}_s$. On the other hand, the spectral density of noise for the heat current at zero frequency is given by

$$S_{\dot{Q}}(0) = \int_{-\infty}^{\infty} dt' \langle \dot{H}_s(t') \dot{H}_s(0) \rangle_0 \quad (47)$$

analogously to what was introduced in tunneling case. After some algebra and a careful comparison of Eqs. (46) and (47) we find the FDT given in Eq. (42).

C. Effective temperature fluctuations

Here we consider a system with varying temperature $T(t)$. This setup, shown in Fig. 2(a), presents an absorber of a calorimeter or bolometer coupled via thermal conductance G_{th} to a heat bath at fixed temperature T_0 . If we further assume that the small system has heat capacity \mathcal{C} , the energy balance equation reads for the heat current $\dot{Q}(t)$ between the bath and the absorber

$$\dot{Q}(t) = \mathcal{C} \dot{T}(t) + G_{\text{th}} \delta T(t), \quad (48)$$

where $\delta T(t)$ is the difference between the absorber temperature and that of the bath. In order to calculate thermal noise, we again evaluate the two-time correlator as

$$\langle \dot{Q}(t) \dot{Q}(0) \rangle = \mathcal{C}^2 \langle \dot{T}(t) \dot{T}(0) \rangle + G_{\text{th}}^2 \langle \delta T(t) \delta T(0) \rangle, \quad (49)$$

leading to

$$S_{\dot{Q}}(\omega) = (\omega^2 \mathcal{C}^2 + G_{\text{th}}^2) S_T(\omega). \quad (50)$$

Since we typically consider frequencies well below the temperature, $S_{\dot{Q}}(\omega)$ is essentially frequency independent, (which was shown by Eq. (41) for tunneling) and the classical FDT holds for $S_{\dot{Q}}(0)$ in form of Eq. (42) in equilibrium. Thus we have

$$S_T(\omega) = \frac{2k_B T_0^2}{G_{\text{th}}} \frac{1}{1 + (\omega\tau)^2}, \quad (51)$$

where $\tau = \mathcal{C}/G_{\text{th}}$ is the thermal relaxation time. This means that at very low frequencies $S_T(0) = 2k_B T^2/G_{\text{th}}$. The root-mean-square (rms) fluctuation of temperature

is obtained as inverse Fourier transform of the noise spectrum at $t = 0$ as

$$\langle \delta T^2 \rangle = \int_{-\infty}^{\infty} \frac{d\omega}{2\pi} S_T(\omega) = \frac{k_B T_0^2}{\mathcal{C}}, \quad (52)$$

which is the well-known textbook result of temperature fluctuations (van den Berg *et al.*, 2015; Heikkilä and Nazarov, 2009; Lifshitz and Pitaevskii, 1980). The results of Eqs. (51) and (52) are directly accessible in experiments.

D. Progress on measuring fluctuations of heat current and entropy

The previous discussion applies for systems and processes in or very near equilibrium. Over the past decades relations holding also far from equilibrium and for finite times have been developed (Bochkov and Kuzovlev, 1981; Crooks, 1999; Jarzynski, 1997; Seifert, 2012). During the past 20 years they have also become experimentally feasible mainly thanks to advances in production and manipulation of nanostructures. The best known non-equilibrium fluctuation relations governing entropy production ΔS are given by $P(\Delta S)/P(-\Delta S) = e^{\Delta S/k_B}$ and its corollary $\langle e^{-\Delta S/k_B} \rangle = 1$. Here $\langle \cdot \rangle$ refers to the average over many experimental realizations or to the expectation value for the measurement. For macroscopic systems near equilibrium these relations simplify into second law of thermodynamics.

Here we give a brief summary of such non-equilibrium experiments on electrical systems. Fluctuations of entropy production and heat currents have been actively studied experimentally for more than a decade in the classical regime, but mainly via indirect means of detection since entropy is a tricky quantity for a direct measurement (Kleeroin *et al.*, 2019). Two main classes of systems under study have been those in the seminal experiments on molecules (Collin *et al.*, 2005) and on electrical circuits (Bérut *et al.*, 2016; Ciliberto *et al.*, 2013; Küng *et al.*, 2012; Pekola, 2015; Saira *et al.*, 2012b). These works go beyond FDT by addressing far-from-equilibrium fluctuation relations (Bochkov and Kuzovlev, 1981; Campisi *et al.*, 2011; Crooks, 1999; Jarzynski, 1997; Pekola and Khaymovich, 2019; Seifert, 2012). In the work by (Ciliberto *et al.*, 2013) as shown in Fig. 19(a), the setup of two macroscopic resistors was examined at temperatures around the ambient. An indirect measurement of entropy was facilitated in (Ciliberto *et al.*, 2013) via the detection of instantaneous electrical power IV , integrated over time and divided by the corresponding temperature of the macroscopic resistor. This way several fluctuation relations for entropy production under non-equilibrium conditions (Seifert, 2005, 2012) could be verified together with the standard FDT in linear response regime. Similarly in the setup of (Saira

et al., 2012b) of Fig. 19(b), detecting single electrons making non-equilibrium transitions across a junction in a single-electron box provides indirect means of observing the dissipated energy and entropy production quantitatively (Averin and Pekola, 2011; Koski *et al.*, 2013). These experiments were performed at temperatures three orders of magnitude lower than in (Ciliberto *et al.*, 2013). The Crooks (Crooks, 1999) and Jarzynski (Jarzynski, 1997) relations as well as generalized relations incorporating the role of information in Maxwell demon setup (Sagawa and Ueda, 2010) could be tested accurately in these experiments (Pekola and Khaymovich, 2019).

The reason for using indirect measurement of heat by detailed electrical characterization is the fact that the powers are far too small to resolve, e.g. by direct thermometry (Section III.B). Next, we focus on progress of direct measurement of heat current fluctuations.

E. Energy sensitivity of a calorimeter

The ultimate energy resolution of a thermal detector, see Fig. 20, is determined by the coupling of it to the heat bath associated with the fluctuations of heat current. Taking a wide band thermometer on a calorimeter, the rms fluctuations of the effective temperature due to this intrinsic noise are given by Eq. (52). In order to find the energy resolution of the detector one needs to compare this noise to the impact of the absorption of energy E on the temperature of the detector, which can be evaluated by solving Eq. (48) for an instantaneous absorption of a photon at energy E at time instant $t = 0$, meaning $\dot{Q}(t) = E\delta(t)$ with the solution $\delta T(t) = (E/C)e^{-t/\tau}\theta(t)$, where the time constant $\tau = C/G_{\text{th}}$ and $\theta(t)$ is the Heaviside step function. Thus at $t = 0+$, the immediate rise of T is $\delta T(0) = E/C$. The signal-to-noise ratio $\text{SNR} = \delta T(0)/\sqrt{\langle \delta T^2 \rangle}$ is

$$\text{SNR} = E/\sqrt{k_{\text{B}}T_0^2\mathcal{C}}, \quad (53)$$

meaning that the energy resolution of the detector in this regime is

$$\delta E = \sqrt{k_{\text{B}}T_0^2\mathcal{C}}. \quad (54)$$

For convenience, let us write $\mathcal{C} = \eta k_{\text{B}}$, where η is a dimensionless constant that we assess below. Then we find that $\delta E = \sqrt{\eta}k_{\text{B}}T_0$. As an example, related to the experiment of (Karimi *et al.*, 2020), we take a metallic calorimeter where $\mathcal{C} = \gamma\mathcal{V}T_0$ at low temperatures (see Fig. 20(a),(b)). Here $\gamma \sim 100 \text{ JK}^{-2}\text{m}^{-3}$ for copper and $\mathcal{V} < 10^{-21} \text{ m}^3$ is the volume of the absorber, yielding $\eta \sim 100$ and energy resolution $\delta E/k_{\text{B}} \sim 0.1 \text{ K}$ at $T_0 = 0.01 \text{ K}$ (Karimi and Pekola, 2020).

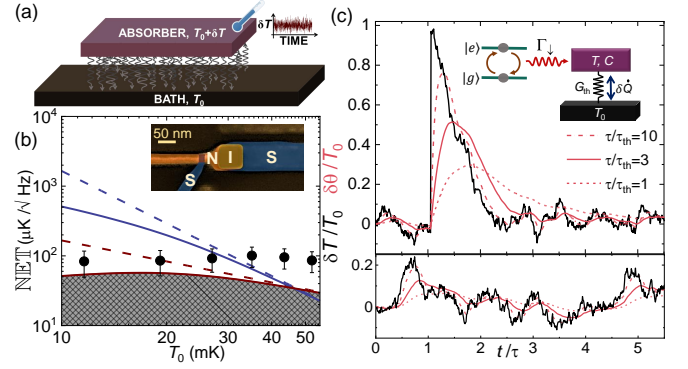


FIG. 20 Quantum calorimeter. (a) A normal-metal absorber is coupled to the phonon heat bath at fixed temperature T_0 via electron-phonon collisions, shown by many arrows. These collisions lead to stochastic exchange of heat between the absorber and the bath, and to fluctuating temperature δT in the absorber. The core of the device is the calorimeter including a thermometer, which measures the temporal temperature variations. An example of a temperature trace is shown next to the absorber. (b) Noise equivalent temperature of the calorimeter. The solid symbols are the measured signal of temperature fluctuations in equilibrium $\text{NET} \equiv \sqrt{S_T} = \sqrt{\langle \delta T^2 \rangle} / (2\Delta f)$ obtained via the measurement of $\langle \delta T^2 \rangle$ with $\Delta f = 10 \text{ kHz}$. The solid and dashed lines represent the noise-equivalent temperature in equilibrium NET, of the normal-metal absorber in the presence and absence of an extra photon contribution, respectively. Red lines (the lower two) display NET in equilibrium $\text{NET}_{\text{eq}} = \sqrt{2k_{\text{B}}T_0^2/G_{\text{th}}}$ while the blue lines (the upper two) show $\text{NET} = \delta\epsilon/\sqrt{\mathcal{C}G_{\text{th}}}$, which is the required NET of a detector to observe a photon with energy $\delta\epsilon = 1 \text{ K} \times k_{\text{B}}$. The prohibited range bordered by the fundamental temperature fluctuations in equilibrium is indicated by the shaded area. (Inset) Scanning electron micrograph of part of the actual sensor, the SNIS structure, where Cu is used as a normal metal N and Al as a superconductor S. The SNIS junction is the dissipative element in the RLC circuit operating at $f_0 \approx 650 \text{ MHz}$. (c) Simulation of the expected thermometer signal of a calorimeter in response to the absorption of an incoming photon depicted in the inset. The parameters of the simulation of the detector correspond to the experiment shown in (b), with $\eta \equiv C/k_{\text{B}} = 100$ and $\hbar\omega_{\text{Q}}/(k_{\text{B}}T_0) = 100$, where $\hbar\omega_{\text{Q}}$ is the qubit energy, and $T_0 = 10 \text{ mK}$. The noise seen in the traces is the result of temperature fluctuations due to the coupling of the absorber to the phonon bath. Upper panel shows a jump occurring at $t/\tau = 1$ (the time instant set arbitrarily) exceeding the noise level of equilibrium fluctuations, with signal-to-noise ratio of about 10. The red lines (truncated by filtering) show the results at different cut-off frequencies of the thermometer, parametrized by the ratio of the electron-phonon time and the detector response time. (a) Adapted from (Karimi *et al.*, 2020) and (b) adapted from (Karimi and Pekola, 2020).

The fluctuations in power have direct impact on the performance of calorimeters and bolometers (Gildemeister *et al.*, 2001; Irwin, 1995), i.e. thermal detectors of radiation. This noise determines the energy resolution of a calorimeter, and also the noise-equivalent power under continuous irradiation, like in the measurement of the

cosmic microwave background (Mather, 1982). Direct measurements of fluctuating temperature are rare ((Chui *et al.*, 1992; Karimi *et al.*, 2020)). The pioneering measurement of (Chui *et al.*, 1992) employed a macroscopic calorimeter working at the so-called lambda point of liquid helium, i.e. its superfluid transition temperature at $T = 2.17$ K. They managed to verify Eqs. (51) and (52) thanks to a very high resolution of the thermometer measuring the magnetization of a paramagnetic salt (copper ammonium bromide) with the help of a SQUID down to 10^{-10} K/ $\sqrt{\text{Hz}}$ noise equivalent temperature.

The nanofabricated detector of (Karimi *et al.*, 2020) worked in the regime where the measurement cut-off frequency was 10 kHz, which falls somewhat below $1/\tau$. Furthermore the metallic absorber was proximitized by a superconducting contact further decreasing C and G_{th} (Heikkilä and Giazotto, 2009; Nikolic *et al.*, 2020) and this way improving its performance. The experiment (Fig. 20(b)), utilizing a SNIS (superconductor-normal metal-insulator-superconductor) thermometer (Karimi and Pekola, 2018) demonstrated noise of the effective temperature of the calorimeter that is very close to the expected fundamental fluctuation limit of Eq. (51) at low frequencies, at the same time promising a SNR of ~ 10 in measuring an absorption event with photon energy $E/k_B = 1$ K. Figure 20(c) demonstrates by simulation the validity of the analysis above. The wide-band detector would present T fluctuations which are an order of magnitude smaller than the temperature jump due to the 1 K photon absorption event. In summary of this measurement, it demonstrates the feasibility of a microwave photon measurement using a metallic calorimeter at $T_0 = 10$ mK.

There exist several other concepts of ultrasensitive thermal detectors, either metallic (Govenius *et al.*, 2016; Kuzmin *et al.*, 2019) or those utilizing graphene or semiconductors (Kokkoniemi *et al.*, 2020, 2019; Lara-Avila *et al.*, 2019; Lee *et al.*, 2020; Roukes, 1999), or those based on, e.g., temperature dependent magnetization (Enss, 2005; Kempf *et al.*, 2018). The advantage of graphene is its supposedly very low heat capacity that could make the thermal response time shorter than in metal detectors. Yet at the time of writing this paper, none of the proposed detectors has demonstrated detection of quanta in the said microwave regime.

XI. SUMMARY AND OUTLOOK

In this review we have focused on fundamental aspects of quantum heat transport, moreover with main emphasis on experiments carried out during the past 20 years. It is probably fair to say that in many respects the physics of heat transport in quantum nanostructures is by now well understood, and experiments tend to confirm the theoretical predictions. In some systems clean experiments

are, however, more difficult to realize than in others from practical point of view, and more experiments are needed: one example among others is presented by the one dimensional phonon structures where beautiful pioneering experiments were performed already long ago (Schwab *et al.*, 2000), but where precise conditions of how to realize ballistic contacts are still under debate. The experiments on quantum heat transport serve also as tools to understand quantum matter itself, like the recent experiments in the fractional quantum Hall regime demonstrate (Banerjee *et al.*, 2017; Dutta *et al.*, 2021). On the other hand they show us ways of realizing new kinds of devices and of how to nail down and achieve their ultimate limits of performance. We discussed the latter issue in Section X on noise in heat current.

As to the potentially useful devices based on quantum heat transport, we discuss briefly two examples. The first one is a rather straightforward application of heat management on-chip for quantum information processes. Microwave photons provide a means to transport quanta and energy in general over large distances as we discussed in Section VII.C. It could thus serve as a way to reset quantum circuits rapidly. There is, however, a trade-off to be considered. Rapid thermalization is almost a synonym for low quality factor and fast decoherence of a quantum system, which are naturally not desirable properties. Therefore tunable coupling is a possible way to go, to switch on and off the coupling to a heat bath on demand. Variations of the many heat valves presented in this article could in principle serve the purpose. Tests of such an idea have been proposed and experimented on in (Partanen *et al.*, 2018).

Quantum heat engines and cyclic refrigerators are presently under intensive study, see, e.g. (Alicki and Kosloff, 2018; Benenti *et al.*, 2017; Brandner *et al.*, 2017; Campisi and Fazio, 2016; Deffner *et al.*, 2014; Humphrey and Linke, 2005; Josefsson *et al.*, 2018; Quan *et al.*, 2007; Raja *et al.*, 2021). Experiments fully in the quantum regime are up to now practically nonexistent, although there are proposals that address realistic setups (Abah *et al.*, 2012; Karimi and Pekola, 2016). For instance, a so-called quantum Otto cycle can be realized by coupling a superconducting qubit alternately to two different heat baths (Karimi and Pekola, 2016). If this is done by varying the energy level separation of the qubit, like was done in the photonic heat valve or rectifier above, but now cyclically at RF frequencies, one can extract heat from the cold bath and dump it to the hot one, when system parameters are chosen properly. We expect devices of this type or analogous ones to work in the near future. Interesting questions arise on whether one can boost up the powers and/or efficiencies by exploiting quantum dynamics, and by what kind of protocols one can speed up the cycles for higher powers in general (Funo *et al.*, 2019; Menczel *et al.*, 2019; Solfanelli *et al.*, 2020).

We want to briefly note here that topological mat-

ter (Hasan and Kane, 2010; Qi and Zhang, 2011), specifically topological superconductors and Josephson junctions, have been proposed as potential novel elements in quantum thermodynamics and heat transport experiments due to their unconventional physical properties, see e.g., non exhaustive list of some recent work in (Bauer and Sothmann, 2019; Pan *et al.*, 2021; Rivas and Martin-Delgado, 2017; Scharf *et al.*, 2020). Due to the focus of the current paper, mainly on experiments, we do not discuss this topic further.

In this review we have alluded to the connections of heat transport and quantum thermodynamics mainly regarding concrete device concepts, including thermal detectors, heat engines and refrigerators. On a more fundamental level, quantum heat transport is in the heart of open quantum systems physics (Breuer and Petruccione, 2002) with non-Hermitian dynamics governed by the quantum noise (Gardiner and Zoller, 2010) widely discussed in this review. True thermodynamics counts on observations of heat currents and temperatures, and power consumption of the sources. Adopting this view, one can pose many questions like how to measure work and heat in an open quantum system, for which the measurement apparatus cannot be viewed as an innocent witness of what is happening in the quantum system itself. The calorimeter can eventually become the microscope of quantum dynamics on the level of exchange of energy by individual quanta emitted or absorbed by the quantum system. This would give us the optimal tool to investigate stochastic thermodynamics in true quantum regime. Many other fundamentally and practically important questions arise and can potentially be answered by heat transport experiments. For instance, how does a quantum system thermalize, and does it find an equilibrium thermal state even in the absence of a heat bath? To conclude, investigations and exploitation of quantum heat transport will play an important role in the currently active field of quantum thermodynamics and in future quantum technologies in general.

XII. ACKNOWLEDGMENTS

This work was supported by Academy of Finland grant 312057, the European Union’s Horizon 2020 research and innovation programme under the Marie Skłodowska-Curie actions (grant agreement 766025), the Russian Science Foundation (Grant No. 20-62-46026), and Foundational Questions Institute Fund (FQXi) via Grant No. FQXi-IAF19-06.

REFERENCES

- Abah, O, J. Roßnagel, G. Jacob, S. Deffner, F. Schmidt-Kaler, K. Singer, and E. Lutz (2012), “Single-ion heat engine at maximum power,” *Phys. Rev. Lett.* **109**, 203006.
- Alicki, Robert, and Ronnie Kosloff (2018), *Thermodynamics in the Quantum Regime: Fundamental Aspects and New Directions*, edited by Felix Binder, Luis A. Correa, Christian Gogolin, Janet Anders, and Gerardo Adesso (Springer).
- Altimiras, C, H. le Sueur, U. Gennser, A. Cavanna, D. Mailly, and F. Pierre (2010), “Tuning energy relaxation along quantum hall channels,” *Phys. Rev. Lett.* **105**, 226804.
- Ashcroft, Neil W, and N. David Mermin (1976), *Solid State Physics* (Holt, Rinehart and Winston).
- Aurell, Erik, and Federica Montana (2019), “Thermal power of heat flow through a qubit,” *Phys. Rev. E* **99**, 042130.
- Averin, D V, and K. K. Likharev (1991), *Mesoscopic phenomena in solids, Single Electronics: A correlated transfer of single electrons and Cooper pairs in systems of small tunnel junctions*, edited by B. L. Altshuler, P. A. Lee, and R. A. Webb (Elsevier Science Publishers B. V.).
- Averin, D V, and J. P. Pekola (2011), “Statistics of the dissipated energy in driven single-electron transitions,” *EPL* **96**, 67004.
- Averin, Dmitri V, and Jukka P. Pekola (2010), “Violation of the fluctuation-dissipation theorem in time-dependent mesoscopic heat transport,” *Phys. Rev. Lett.* **104**, 220601.
- Banerjee, Mitali, Moty Heiblum, Amir Rosenblatt, Yuval Oreg, Dima E. Feldman, Ady Stern, and Vladimir Umansky (2017), “Observed quantization of anyonic heat flow,” *Nature* **545**, 75–79.
- Banerjee, Mitali, Moty Heiblum, Vladimir Umansky, Dima E. Feldman, Yuval Oreg, and Ady Stern (2018), “Observation of half-integer thermal hall conductance,” *Nature* **559**, 205.
- Bardeen, J, L. N. Cooper, and J. R. Schrieffer (1957), “Theory of superconductivity,” *Phys. Rev.* **108**, 1175–1204.
- Bardeen, J, G. Rickayzen, and L. Tewordt (1959), “Theory of the thermal conductivity of superconductors,” *Phys. Rev.* **113**, 982–994.
- Bauer, Alexander G, and Björn Sothmann (2019), “Phase-dependent heat transport in Josephson junctions with p -wave superconductors and superfluids,” *Phys. Rev. B* **99**, 214508.
- Benenti, Giuliano, Giulio Casati, Keiji Saito, and Robert S. Whitney (2017), “Fundamental aspects of steady-state conversion of heat to work at the nanoscale,” *Physics Reports* **694**, 1 – 124.
- van den Berg, Tineke L, Fredrik Brange, and Peter Samuelsson (2015), “Energy and temperature fluctuations in the single electron box,” *New Journal of Physics* **17** (7), 075012.
- Bhandari, Bibek, Paolo Andrea Erdman, Rosario Fazio, Elisabetta Paladino, and Fabio Taddei (2021), “Thermal rectification through a nonlinear quantum resonator,” *Phys. Rev. B* **103**, 155434.
- Blencowe, Miles P, and Vincenzo Vitelli (2000), “Universal quantum limits on single-channel information, entropy, and heat flow,” *Phys. Rev. A* **62**, 052104.
- Bochkov, GN, and Yu.E. Kuzovlev (1981), “Nonlinear fluctuation-dissipation relations and stochastic models in nonequilibrium thermodynamics: I. generalized fluctuation-dissipation theorem,” *Physica A: Statistical Mechanics and its Applications* **106** (3), 443 – 479.
- Brandner, Kay, Michael Bauer, and Udo Seifert (2017), “Universal coherence-induced power losses of quantum heat engines in linear response,” *Phys. Rev. Lett.* **119**, 170602.
- Breuer, H-P, and F. Petruccione (2002), *The theory of open quantum systems* (Oxford University Press).

- Bérut, A, A. Imparato, A. Petrosyan, and S. Ciliberto (2016), “The role of coupling on the statistical properties of the energy fluxes between stochastic systems at different temperatures,” *J. Stat. Mech.*, 054002.
- Bruus, Henrik, and Karsten Flensberg (2004), *Many-body Quantum Theory in Condensed Matter Physics* (Oxford University Press).
- Butcher, P N (1990), “Thermal and electrical transport formalism for electronic microstructures with many terminals,” *Journal of Physics: Condensed Matter* **2** (22), 4869–4878.
- Callen, Herbert B, and Theodore A. Welton (1951), “Irreversibility and generalized noise,” *Phys. Rev.* **83**, 34–40.
- Campisi, Michele, and Rosario Fazio (2016), “The power of a critical heat engine,” *Nat. Commun.* **7**, 11895.
- Campisi, Michele, Peter Hänggi, and Peter Talkner (2011), “Colloquium: Quantum fluctuation relations: Foundations and applications,” *Rev. Mod. Phys.* **83**, 771–791.
- Chang, C W, D. Okawa, A. Majumdar, and A. Zettl (2006), “Solid-state thermal rectifier,” *Science* **314**, 1121–1124.
- Chang, Yu-Cheng, Bayan Karimi, Jordan Senior, Alberto Ronzani, Joonas T. Peltonen, Hsi-Sheng Goan, Chii-Dong Chen, and Jukka P. Pekola (2019), “Utilization of the superconducting transition for characterizing low-quality-factor superconducting resonators,” *Applied Physics Letters* **115** (2), 022601, <https://doi.org/10.1063/1.5098310>.
- Chiara, Gabriele De, Gabriel Landi, Adam Hewgill, Brendan Reid, Alessandro Ferraro, Augusto J Roncaglia, and Mauro Antezza (2018), “Reconciliation of quantum local master equations with thermodynamics,” *New Journal of Physics* **20** (11), 113024.
- Chiatti, O, J. T. Nicholls, Y. Y. Proskuryakov, N. Lumpkin, I. Farrer, and D. A. Ritchie (2006), “Quantum thermal conductance of electrons in a one-dimensional wire,” *Phys. Rev. Lett.* **97**, 056601.
- Chui, T C P, D. R. Swanson, M. J. Adriaans, J. A. Nissen, and J. A. Lipa (1992), “Temperature fluctuations in the canonical ensemble,” *Phys. Rev. Lett.* **69**, 3005–3008.
- Ciliberto, S, A. Imparato, A. Naert, and M. Tanase (2013), “Heat flux and entropy produced by thermal fluctuations,” *Phys. Rev. Lett.* **110**, 180601.
- Clark, A M, A. Williams, S. T. Ruggiero, M. L. van den Berg, and J. N. Ullom (2004), “Practical electron-tunneling refrigerator,” *Applied Physics Letters* **84**, 625–627.
- Clarke, John, and Frank K. Wilhelm (2008), “Superconducting quantum bits,” *Nature* **453**, 1031–1042.
- Collin, D, F. Ritort, C. Jarzynski, S. B. Smith, I. Tinoco Jr, and C. Bustamante (2005), “Verification of the crooks fluctuation theorem and recovery of rna folding free energies,” *Nature* **437**, 231–234.
- Courtois, H, F. W. J. Hekking, H. Q. Nguyen, and C. B. Winkelmann (2014), “Electronic coolers based on superconducting tunnel junctions: Fundamentals and applications,” *J. Low Temp. Phys.* **175**, 799–812.
- Crépieux, A (2021), “Electronic heat current fluctuations in a quantum dot,” *Phys. Rev. B* **103**, 045427.
- Crooks, Gavin E (1999), “Entropy production fluctuation theorem and the nonequilibrium work relation for free energy differences,” *Phys. Rev. E* **60**, 2721–2726.
- Cui, Longji, Wonho Jeong, Sunghoon Hur, Manuel Matt, Jan C. Klöckner, Fabian Pauly, Peter Nielaba, Juan Carlos Cuevas, Edgar Meyhofer, and Pramod Reddy (2017), “Quantized thermal transport in single-atom junctions,” *Science* **355** (6330), 1192–1195.
- Deffner, Sebastian, Christopher Jarzynski, and Adolfo del Campo (2014), “Classical and quantum shortcuts to adiabaticity for scale-invariant driving,” *Phys. Rev. X* **4**, 021013.
- Donvil, Brecht, Paolo Muratore-Ginanneschi, and Dmitry Golubev (2020), “Exactly solvable model of calorimetric measurements,” *Phys. Rev. B* **102**, 245401.
- Donvil, Brecht, Paolo Muratore-Ginanneschi, Jukka P. Pekola, and Kay Schwieger (2018), “Model for calorimetric measurements in an open quantum system,” *Phys. Rev. A* **97**, 052107.
- Dutta, B, J. T. Peltonen, D. S. Antonenko, M. Meschke, M. A. Skvortsov, B. Kubala, J. König, C. B. Winkelmann, H. Courtois, and J. P. Pekola (2017), “Thermal conductance of a single-electron transistor,” *Phys. Rev. Lett.* **119**, 077701.
- Dutta, Bivas, Wenmin Yang, Ron Aharon Melcer, Hemanta Kumar Kundu, Moty Heiblum, Vladimir Umansky, Yuval Oreg, Ady Stern, and David Mross (2021), “Novel method distinguishing between competing topological orders,” [arXiv:2101.01419](https://arxiv.org/abs/2101.01419) <https://arxiv.org/abs/2101.01419>.
- Enss, Christian, Ed. (2005), *Cryogenic Particle Detection* (Springer Berlin Heidelberg).
- Feshchenko, A V, J. V. Koski, and J. P. Pekola (2014), “Experimental realization of a coulomb blockade refrigerator,” *Phys. Rev. B* **90**, 201407.
- Feshchenko, A V, O.-P. Saira, J. T. Peltonen, and J. P. Pekola (2017), “Thermal conductance of nb thin films at sub-kelvin temperatures,” *Sci. Rep.* **7**, 41728.
- Fleischmann, A, A. Reiser, and C. Enss (2020), “Noise thermometry for ultralow temperatures,” *J. Low Temp. Phys.* **201**, 803–824.
- Funo, Ken, Neill Lambert, Bayan Karimi, Jukka P. Pekola, Yuta Masuyama, and Franco Nori (2019), “Speeding up a quantum refrigerator via counterdiabatic driving,” *Phys. Rev. B* **100**, 035407.
- Gantmakher, V F (1974), “The experimental study of electron-phonon scattering in metals,” *Rep. Prog. Phys.* **37** (3), 317.
- Gardiner, C W, and P. Zoller (2010), *Quantum Noise* (Springer-Verlag Berlin Heidelberg).
- Giazotto, Francesco, Tero T. Heikkilä, Arttu Luukanen, Alexander M. Savin, and Jukka P. Pekola (2006), “Opportunities for mesoscopies in thermometry and refrigeration: Physics and applications,” *Rev. Mod. Phys.* **78**, 217–274.
- Giazotto, Francesco, and María José Martínez-Pérez (2012), “The josephson heat interferometer,” *Nature* **492**, 401–405.
- Gildemeister, Jan M, Adrian T. Lee, and Paul L. Richards (2001), “Model for excess noise in voltage-biased superconducting bolometers,” *Appl. Opt.* **40** (34), 6229–6235.
- Golubev, D S, and J. P. Pekola (2015), “Statistics of heat exchange between two resistors,” *Phys. Rev. B* **92**, 085412.
- Golubev, Dmitry, Timothé Faivre, and Jukka P. Pekola (2013), “Heat transport through a josephson junction,” *Phys. Rev. B* **87**, 094522.
- Goury, Donald, and Rafael Sánchez (2019), “Reversible thermal diode and energy harvester with a superconducting quantum interference single-electron transistor,” *Appl. Phys. Lett.* **115**, 092601.
- Govenius, J, R. E. Lake, K. Y. Tan, and M. Möttönen (2016), “Detection of zeptojoule microwave pulses using electrothermal feedback in proximity-induced josephson junctions,” *Phys. Rev. Lett.* **117**, 030802.

- Granger, G, J. P. Eisenstein, and J. L. Reno (2009), “Observation of chiral heat transport in the quantum hall regime,” *Phys. Rev. Lett.* **102**, 086803.
- Guttman, Glen D, Eshel Ben-Jacob, and David J. Bergman (1998), “Interference effect heat conductance in a josephson junction and its detection in an rf squid,” *Phys. Rev. B* **57**, 2717–2719.
- Guttman, Glen D, Benny Nathanson, Eshel Ben-Jacob, and David J. Bergman (1997), “Phase-dependent thermal transport in josephson junctions,” *Phys. Rev. B* **55**, 3849–3855.
- Halbental, D, J. Cuppens, M. Ben Shalom, L. Embon, N. Shadmi, Y. Anahory, H. R. Naren, J. Sarkar, A. Uri, Y. Ronen, Y. Myasoedov, L. S. Levitov, E. Joselevich, A. K. Geim, and E. Zeldov (2016), “Nanoscale thermal imaging of dissipation in quantum systems,” *Nature* **539**, 407.
- Halbental, Dorri, Moshe Ben Shalom, Aviram Uri, Kousik Bagani, Alexander Y. Meltzer, Ido Marcus, Yuri Myasoedov, John Birkbeck, Leonid S. Levitov, Andre K. Geim, and Eli Zeldov (2017), “Imaging resonant dissipation from individual atomic defects in graphene,” *Science* **358**, 1303.
- Hasan, M Z, and C. L. Kane (2010), “Colloquium: Topological insulators,” *Rev. Mod. Phys.* **82**, 3045–3067.
- Heikkilä, T T, and Francesco Giazotto (2009), “Phase sensitive electron-phonon coupling in a superconducting proximity structure,” *Phys. Rev. B* **79**, 094514.
- Heikkilä, T T, and Yuli V. Nazarov (2009), “Statistics of temperature fluctuations in an electron system out of equilibrium,” *Phys. Rev. Lett.* **102**, 130605.
- Hewgill, Adam, Gabriele De Chiara, and Alberto Imparato (2020), “Quantum thermodynamically consistent local master equations,” arXiv:2008.04742.
- Hofer, Patrick P, Marti Perarnau-Llobet, L David M Miranda, Géraldine Haack, Ralph Silva, Jonatan Bohr Brask, and Nicolas Brunner (2017), “Markovian master equations for quantum thermal machines: local versus global approach,” *New Journal of Physics* **19** (12), 123037.
- Humphrey, TE, and H. Linke (2005), “Quantum, cyclic, and particle-exchange heat engines,” *Physica E: Low-dimensional Systems and Nanostructures* **29** (1), 390 – 398, *frontiers of Quantum*.
- Iorio, A, E. Strambini, G. Haack, M. Campisi, and F. Giazotto (2021), “Photonic heat rectification in a system of coupled qubits,” *Phys. Rev. Applied* **15**, 054050.
- Irwin, K D (1995), “An application of electrothermal feedback for high resolution cryogenic particle detection,” *Appl. Phys. Lett.* **66**, 1998.
- Jarzynski, C (1997), “Nonequilibrium equality for free energy differences,” *Phys. Rev. Lett.* **78**, 2690–2693.
- Jezouin, S, F. D. Parmentier, A. Anthore, U. Gennser, A. Cavanna, Y. Jin, and F. Pierre (2013), “Quantum limit of heat flow across a single electronic channel,” *Science* **342**, 601–604.
- Johnson, J B (1928), “Thermal agitation of electricity in conductors,” *Phys. Rev.* **32**, 97–109.
- Josefsson, Martin, Artis Svilans, Adam M. Burke, Eric A. Hoffmann, Sofia Fahlvik, Claes Thelander, Martin Leijnse, and Heiner Linke (2018), “A quantum-dot heat engine operating close to the thermodynamic efficiency limits,” *Nat. Nanotechnol.* **13**, 920.
- Josephson, BD (1962), “Possible new effects in superconductive tunnelling,” *Physics Letters* **1** (7), 251 – 253.
- Kane, C L, and Matthew P. A. Fisher (1997), “Quantized thermal transport in the fractional quantum hall effect,” *Phys. Rev. B* **55**, 15832–15837.
- Kargı, Cahit, M. Tahir Naseem, Tomáš Opatrný, Özgür E. Müstecaplıoğlu, and Gershon Kurizki (2019), “Quantum optical two-atom thermal diode,” *Phys. Rev. E* **99**, 042121.
- Karimi, B, and J. P. Pekola (2016), “Otto refrigerator based on a superconducting qubit: Classical and quantum performance,” *Phys. Rev. B* **94**, 184503.
- Karimi, Bayan, Fredrik Brange, Peter Samuelsson, and Jukka P. Pekola (2020), “Reaching the ultimate energy resolution of a quantum detector,” *Nat. Commun.* **11**, 367.
- Karimi, Bayan, and Jukka P. Pekola (2018), “Noninvasive thermometer based on the zero-bias anomaly of a superconducting junction for ultrasensitive calorimetry,” *Phys. Rev. Applied* **10**, 054048.
- Karimi, Bayan, and Jukka P. Pekola (2020), “Quantum trajectory analysis of single microwave photon detection by nanocalorimetry,” *Phys. Rev. Lett.* **124**, 170601.
- Karimi, Bayan, and Jukka P. Pekola (2021), “Down-conversion of quantum fluctuations of photonic heat current in a circuit,” arXiv:2104.09238.
- Kempf, S, A. Fleischmann, L. Gastaldo, and C. Enss (2018), “Physics and applications of metallic magnetic calorimeters,” *J. Low Temp. Phys.* **193**, 365–379.
- Kjaergaard, Morten, Mollie E. Schwartz, Jochen Braumüller, Philip Krantz, Joel I.-J. Wang, Simon Gustavsson, and William D. Oliver (2020), “Superconducting qubits: Current state of play,” *Annual Review of Condensed Matter Physics* **11** (1), 369–395.
- Kleorin, Yaakov, Holger Thierschmann, Hartmut Buhmann, Antoine Georges, Laurens W. Molenkamp, and Yigal Meir (2019), “How to measure the entropy of a mesoscopic system via thermoelectric transport,” *Nat. Commun.* **10**, 5801.
- Koch, Jens, Terri M. Yu, Jay Gambetta, A. A. Houck, D. I. Schuster, J. Majer, Alexandre Blais, M. H. Devoret, S. M. Girvin, and R. J. Schoelkopf (2007), “Charge-insensitive qubit design derived from the cooper pair box,” *Phys. Rev. A* **76**, 042319.
- Kokkonen, R, J.-P. Girard, D. Hazra, A. Laitinen, J. Govenius, R. E. Lake, I. Sallinen, V. Vesterinen, M. Partanen, J. Y. Tan, K. W. Chan, K. Y. Tan, P. Hakonen, and M. Möttönen (2020), “Bolometer operating at the threshold for circuit quantum electrodynamics,” *Nature* **586**, pages47–51.
- Kokkonen, Roope, Joonas Govenius, Visa Vesterinen, Russell E. Lake, András M. Gunyhó, Kuan Y. Tan, Slawomir Simbierowicz, Leif Grönberg, Janne Lehtinen, Mika Prunnila, Juha Hassel, Antti Lamminen, Olli-Pentti Saira, and Mikko Möttönen (2019), “Nanobolometer with ultralow noise equivalent power,” *Commun. Phys.* **2**, 124.
- Koski, J V, T. Sagawa, O-P. Saira, Y. Yoon, A. Kutvonen, P. Solinas, M. Möttönen, T. Ala-Nissila, and J. P. Pekola (2013), “Distribution of entropy production in a single-electron box,” *Nat. Phys.* **9**, 644–648.
- Krantz, P, M. Kjaergaard, F. Yan, T. P. Orlando, S. Gustavsson, and W. D. Oliver (2019), “A quantum engineer’s guide to superconducting qubits,” *Appl. Phys. Rev.* **6**, 021318.
- Kubala, Björn, Jürgen König, and Jukka Pekola (2008), “Violation of the wiedemann-franz law in a single-electron transistor,” *Phys. Rev. Lett.* **100**, 066801.
- Kubo, Ryogo (1957), “Statistical-mechanical theory of irreversible processes. i. general theory and simple applications to magnetic and conduction problems,” *J. Phys. Soc. Jpn.*

- 12**, 570–586.
- Küing, B, C. Rössler, M. Beck, M. Marthaler, D. S. Golubev, Y. Utsumi, T. Ihn, and K. Ensslin (2012), “Irreversibility on the level of single-electron tunneling,” *Phys. Rev. X* **2**, 011001.
- Kuzmin, L, I Agulo, M Fominsky, A Savin, and M Tarasov (2004), “Optimization of electron cooling by SIN tunnel junctions,” *Superconductor Science and Technology* **17** (5), S400–S405.
- Kuzmin, L S, A. L. Pankratov, A. V. Gordeeva, V. O. Zbrozhek, V. A. Shamporov, L. S. Revin, A. V. Blagodatkin, S. Masi, and P. de Bernardis (2019), “Photon-noise-limited cold-electron bolometer based on strong electron self-cooling for high-performance cosmology missions,” *Commun. Phys.* **2**, 104.
- Landauer, Rolf (1981), “Can a length of perfect conductor have a resistance?” *Phys. Lett.* **85A** (2), 91.
- Lara-Avila, S, A. Danilov, D. Golubev, H. He, K. H. Kim, R. Yakimova, F. Lombardi, T. Bauch, S. Cherednichenko, and S. Kubatkin (2019), “Towards quantum-limited coherent detection of terahertz waves in charge-neutral graphene,” *Nat. Astron.* **3**, 983–988.
- Lee, Gil-Ho, Dmitri K. Efetov, Woonchan Jung, Leonardo Ranzani, Evan D. Walsh, Thomas A. Ohki, Takashi Taniguchi, Kenji Watanabe, Philip Kim, Dirk Englund, and Kin Chung Fong (2020), “Graphene-based josephson junction microwave bolometer,” *Nature* **586**, 42–46.
- Leivo, M M, and J. P. Pekola (1998), “Thermal characteristics of silicon nitride membranes at sub-kelvin temperatures,” *Appl. Phys. Lett.* **72**, 1305.
- Leivo, M M, J. P. Pekola, and D. V. Averin (1996), “Efficient peltier refrigeration by a pair of normal metal/insulator/superconductor junctions,” *Appl. Phys. Lett.* **68**, 1996.
- Leivo, Mikko (1999), “On-chip cooling by quasiparticle tunneling below 1 kelvin,” PhD thesis.
- Levy, Amikam, and Ronnie Kosloff (2014), “The local approach to quantum transport may violate the second law of thermodynamics,” *EPL (Europhysics Letters)* **107** (2), 20004.
- Lifshitz, E M, and L. P. Pitaevskii (1980), *Statistical physics, Part I*, 3rd ed. (Pergamon Press).
- Lounasmaa, O V (1974), *Experimental Principles and Methods Below 1K* (Academic Press).
- Magazzù, L, and M Grifoni (2019), “Transmission spectra of an ultrastrongly coupled qubit-dissipative resonator system,” *Journal of Statistical Mechanics: Theory and Experiment* **2019** (10), 104002.
- Maillet, Olivier, Diego Subero, Joonas T. Peltonen, Dmitry S. Golubev, and Jukka P. Pekola (2020), “Electric field control of radiative heat transfer in a superconducting circuit,” *Nat. Commun.* **11**, 4326.
- Majidi, D, M. Josefsson, M. Kumar, M. Leijnse, L. Samuelson, H. Courtois, C. B. Winkelmann, and V. F. Maisi (2021), “Quantum confinement suppressing electronic heat flow below the wiedemann-franz law,” arXiv:2106.06229.
- Maki, Kazumi, and Allan Griffin (1965), “Entropy transport between two superconductors by electron tunneling,” *Phys. Rev. Lett.* **15**, 921–923.
- Manninen, A J, M. M. Leivo, and J. P. Pekola (1997), “Refrigeration of a dielectric membrane by superconductor/insulator/normal-metal/insulator/superconductor tunneling,” *Appl. Phys. Lett.* **70**, 1885.
- Martínez-Pérez, Maria José, Antonio Fornieri, and Francesco Giazotto (2015), “Rectification of electronic heat current by a hybridthermal diode,” *Nature Nanotech.* **10**, 303–307.
- Masuda, Shumpei, Kuan Y. Tan, Matti Partanen, Russell E. Lake, Joonas Govenius, Matti Silveri, Hermann Grabert, and Mikko Möttönen (2018), “Observation of microwave absorption and emission from incoherent electron tunneling through a normal-metal–insulator–superconductor junction,” *Sci. Rep.* **8**, 3966.
- Mather, John C (1982), “Bolometer noise: nonequilibrium theory,” *Appl. Opt.* **21** (6), 1125–1129.
- Menczel, Paul, Tuomas Pyhäranta, Christian Flindt, and Kay Brandner (2019), “Two-stroke optimization scheme for mesoscopic refrigerators,” *Phys. Rev. B* **99**, 224306.
- Meschke, Matthias, Wiebke Guichard, and Jukka P. Pekola (2006), “Single-mode heat conduction by photons,” *Nature* **444**, 187–190.
- Molenkamp, L W, Th. Gravier, H. van Houten, O. J. A. Buijk, M. A. A. Mabesoone, and C. T. Foxon (1992), “Peltier coefficient and thermal conductance of a quantum point contact,” *Phys. Rev. Lett.* **68**, 3765–3768.
- Moskalets, Michael (2014), “Floquet scattering matrix theory of heat fluctuations in dynamical quantum conductors,” *Phys. Rev. Lett.* **112**, 206801.
- Mosso, Nico, Ute Drechsler, Fabian Menges, Peter Nirmalraj, Siegfried Karg, Heike Riel, and Bernd Gotsmann (2017), “Heat transport through atomic contacts,” *Nature Nanotechnology* **12**, 430–433.
- Motz, T, M Wiedmann, J T Stockburger, and J Ankerhold (2018), “Rectification of heat currents across nonlinear quantum chains: a versatile approach beyond weak thermal contact,” *New Journal of Physics* **20** (11), 113020.
- Muhonen, Juha T, Matthias Meschke, and Jukka P Pekola (2012), “Micrometre-scale refrigerators,” *Reports on Progress in Physics* **75** (4), 046501.
- Nahum, M, T. M. Eiles, and John M. Martinis (1994), “Electronic microrefrigerator based on a normal-insulator-superconductor tunnel junction,” *Appl. Phys. Lett.* **65**, 3123.
- Nakamura, Y, Yu. A. Pashkin, and J. S. Tsai (1999), “Coherent control of macroscopic quantum states in a single-cooper-pair box,” *Nature* **398**, 786–788.
- Nam, Seung-Geol, E. H. Hwang, and Hu-Jong Lee (2013), “Thermoelectric detection of chiral heat transport in graphene in the quantum hall regime,” *Phys. Rev. Lett.* **110**, 226801.
- Nguyen, H Q, T Aref, V J Kauppila, M Meschke, C B Winkelmann, H Courtois, and J P Pekola (2013), “Trapping hot quasi-particles in a high-power superconducting electronic cooler,” *New Journal of Physics* **15**, 085013.
- Nikolic, Danilo, Denis M. Basko, and Wolfgang Belzig (2020), “Electron cooling by phonons in superconducting proximity structures,” *Phys. Rev. B* **102**, 214514.
- Nyquist, H (1928), “Thermal agitation of electric charge in conductors,” *Phys. Rev.* **32**, 110–113.
- Pan, Haining, Jay D. Sau, and S. Das Sarma (2021), “Three-terminal nonlocal conductance in majorana nanowires: Distinguishing topological and trivial in realistic systems with disorder and inhomogeneous potential,” *Phys. Rev. B* **103**, 014513.
- Partanen, M, K. Y. Tan, J. Govenius, R. E. Lake, M. K. Mäkelä, T. Tantt, and M. Möttönen (2016), “Quantum-limited heat conduction over macroscopic distances,” *Nat. Phys.* **12**, 460.

- Partanen, M, K. Y. Tan, S. Masuda, J. Govenius, R. E. Lake, M. Jenei, L. Grönberg, J. Hassel, S. Simbierowicz, V. Vesterinen, J. Tuorila, T. Ala-Nissila, and M. Möttönen (2018), “Flux-tunable heat sink for quantum electric circuits,” *Sci. Rep.* **8**, 6325.
- Pascal, L M A, H. Courtois, and F. W. J. Hekking (2011), “Circuit approach to photonic heat transport,” *Phys. Rev. B* **83**, 125113.
- Pekola, JP, and I.M. Khaymovich (2019), “Thermodynamics in single-electron circuits and superconducting qubits,” *Annual Review of Condensed Matter Physics* **10** (1), 193–212.
- Pekola, Jukka P (2015), “Towards quantum thermodynamics in electronic circuits,” *Nat. Phys.* **11**, 118–123.
- Pekola, Jukka P, and Bayan Karimi (2018), “Quantum noise of electron–phonon heat current,” *J. Low Temp. Phys.* **191**, 373–379.
- Pekola, Jukka P, and Bayan Karimi (2020), “Qubit decay in circuit quantum thermodynamics,” arXiv:2010.11122 <https://arxiv.org/abs/2010.11122>
- Peltonen, J T, P. Virtanen, M. Meschke, J. V. Koski, T. T. Heikkilä, and J. P. Pekola (2010), “Thermal conductance by the inverse proximity effect in a superconductor,” *Phys. Rev. Lett.* **105**, 097004.
- Pendry, J (1983), “Quantum limits to the flow of information and entropy,” *Journal of Physics A* **16**, 2161–2171.
- Pothier, H, S. Guéron, Norman O. Birge, D. Esteve, and M. H. Devoret (1997), “Energy distribution function of quasiparticles in mesoscopic wires,” *Phys. Rev. Lett.* **79**, 3490–3493.
- Prance, J R, C. G. Smith, J. P. Griffiths, S. J. Chorley, D. Anderson, G. A. C. Jones, I. Farrer, and D. A. Ritchie (2009), “Electronic refrigeration of a two-dimensional electron gas,” *Phys. Rev. Lett.* **102**, 146602.
- Qi, Xiao-Liang, and Shou-Cheng Zhang (2011), “Topological insulators and superconductors,” *Rev. Mod. Phys.* **83**, 1057–1110.
- Quan, H T, Yu-xi Liu, C. P. Sun, and Franco Nori (2007), “Quantum thermodynamic cycles and quantum heat engines,” *Phys. Rev. E* **76**, 031105.
- Raja, S Hamedani, S Maniscalco, G S Paraoanu, J P Pekola, and N Lo Gullo (2021), “Finite-time quantum stirling heat engine,” *New Journal of Physics* **23** (3), 033034.
- Rego, Luis G C, and George Kirczenow (1998), “Quantized thermal conductance of dielectric quantum wires,” *Phys. Rev. Lett.* **81**, 232–235.
- Rego, Luis G C, and George Kirczenow (1999), “Fractional exclusion statistics and the universal quantum of thermal conductance: A unifying approach,” *Phys. Rev. B* **59**, 13080–13086.
- Riera-Campeny, Andreu, Mohammad Mehboudi, Marisa Pons, and Anna Sanpera (2019), “Dynamically induced heat rectification in quantum systems,” *Phys. Rev. E* **99**, 032126.
- Rivas, Ángel, and Miguel A. Martin-Delgado (2017), “Topological heat transport and symmetry-protected boson currents,” *Sci. Rep.* **7**, 6350.
- Rivas, Ángel, A. Douglas K. Plato, Susana F. Huelga, and Martin B. Plenio (2010), “Markovian master equations: a critical study,” *New Journal of Physics* **12** (11), 113032.
- Ronzani, Alberto, Bayan Karimi, Jorden Senior, Yu-Cheng Chang, Joonas T. Peltonen, ChiiDong Chen, and Jukka P. Pekola (2018), “Tunable photonic heat transport in a quantum heat valve,” *Nat. Phys.* **14**, 991.
- Roukes, M L, M. R. Freeman, R. S. Germain, R. C. Richardson, and M. B. Ketchen (1985), “Hot electrons and energy transport in metals at millikelvin temperatures,” *Phys. Rev. Lett.* **55**, 422–425.
- Roukes, ML (1999), “Yoctocalorimetry: phonon counting in nanostructures,” *Physica B: Condensed Matter* **263–264**, 1–15.
- Ruokola, Tomi, Teemu Ojanen, and Antti-Pekka Jauho (2009), “Thermal rectification in nonlinear quantum circuits,” *Phys. Rev. B* **79**, 144306.
- Sagawa, Takahiro, and Masahito Ueda (2010), “Generalized jarzynski equality under nonequilibrium feedback control,” *Phys. Rev. Lett.* **104**, 090602.
- Saira, O-P, A. Kemppinen, V. F. Maisi, and J. P. Pekola (2012a), “Vanishing quasiparticle density in a hybrid al/cu/al single-electron transistor,” *Phys. Rev. B* **85**, 012504.
- Saira, O-P, Y. Yoon, T. Tanttu, M. Möttönen, D. V. Averin, and J. P. Pekola (2012b), “Test of the jarzynski and crooks fluctuation relations in an electronic system,” *Phys. Rev. Lett.* **109**, 180601.
- Saira, Olli-Pentti, Matthias Meschke, Francesco Giazotto, Alexander M. Savin, Mikko Möttönen, and Jukka P. Pekola (2007), “Heat transistor: Demonstration of gate-controlled electronic refrigeration,” *Phys. Rev. Lett.* **99**, 027203.
- Sánchez, Rafael, and Markus Büttiker (2012), “Detection of single-electron heat transfer statistics,” *EPL (Europhysics Letters)* **100** (4), 47008.
- Sánchez, Rafael, Björn Sothmann, and Andrew N Jordan (2015), “Heat diode and engine based on quantum hall edge states,” *New Journal of Physics* **17** (7), 075006.
- Santamore, D H, and M. C. Cross (2001), “Effect of surface roughness on the universal thermal conductance,” *Phys. Rev. B* **63**, 184306.
- Scharf, Benedikt, Alessandro Braggio, Elia Strambini, Francesco Giazotto, and Ewelina M. Hankiewicz (2020), “Topological josephson heat engine,” *Commun. Phys.* **3**, 198.
- Scheibner, R, M König, D Reuter, A D Wieck, C Gould, H Buhmann, and L W Molenkamp (2008), “Quantum dot as thermal rectifier,” *New Journal of Physics* **10**, 083016.
- Schmidt, D R, R. J. Schoelkopf, and A. N. Cleland (2004), “Photon-mediated thermal relaxation of electrons in nanostructures,” *Phys. Rev. Lett.* **93**, 045901.
- Schwab, K. E. A. Henriksen, J. M. Worlock, and M. L. Roukes (2000), “Measurement of the quantum of thermal conductance,” *Nature* **404**, 974–977.
- Segal, Dvira, and Abraham Nitzan (2005), “Spin-boson thermal rectifier,” *Phys. Rev. Lett.* **94**, 034301.
- Seifert, Udo (2005), “Entropy production along a stochastic trajectory and an integral fluctuation theorem,” *Phys. Rev. Lett.* **95**, 040602.
- Seifert, Udo (2012), “Stochastic thermodynamics, fluctuation theorems and molecular machines,” *Reports on Progress in Physics* **75** (12), 126001.
- Senior, Jorden, Azat Gubaydullin, Bayan Karimi, Joonas T. Peltonen, Joachim Ankerhold, and Jukka P. Pekola (2020), “Heat rectification via a superconducting artificial atom,” *Commun. Phys.* **3**, 40.
- Sergi, Danilo (2011), “Energy transport and fluctuations in small conductors,” *Phys. Rev. B* **83**, 033401.
- Silveri, Matti, Hermann Grabert, Shumpei Masuda, Kuan Yen Tan, and Mikko Möttönen (2017), “Theory of quantum-circuit refrigeration by photon-assisted electron

- tunneling,” *Phys. Rev. B* **96**, 094524.
- Sivan, U, and Y. Imry (1986), “Multichannel landauer formula for thermoelectric transport with application to thermopower near the mobility edge,” *Phys. Rev. B* **33**, 551–558.
- Sivre, E, A. Anthore, F. D. Parmentier, A. Cavanna, U. Gennser, A. Ouerghi, Y. Jin, and F. Pierre (2018), “Heat coulomb blockade of one ballistic channel,” *Nat. Phys.* **14**, 145.
- Solfanelli, Andrea, Marco Falsetti, and Michele Campisi (2020), “Nonadiabatic single-qubit quantum otto engine,” *Phys. Rev. B* **101**, 054513.
- Sothmann, Björn, Rafael Sánchez, Andrew N. Jordan, and Markus Büttiker (2012), “Rectification of thermal fluctuations in a chaotic cavity heat engine,” *Phys. Rev. B* **85**, 205301.
- le Sueur, H, C. Altimiras, U. Gennser, A. Cavanna, D. Mailly, and F. Pierre (2010), “Energy relaxation in the integer quantum hall regime,” *Phys. Rev. Lett.* **105**, 056803.
- Tan, Kuan Yen, Matti Partanen, Russell E. Lake, Joonas Govenius, Shumpei Masuda, and Mikko Möttönen (2017), “Quantum-circuit refrigerator,” *Nat. Commun.* **8**, 15189.
- Tavakoli, Adib, Christophe Blanc, Hossein Ftouni, Kunal J. Lulla, Andrew D. Fefferman, Eddy Collin, and Olivier Bourgeois (2017), “Universality of thermal transport in amorphous nanowires at low temperatures,” *Phys. Rev. B* **95**, 165411.
- Tavakoli, Adib, Kunal Lulla, Thierry Crozes, Natalio Mingo, Eddy Collin, and Olivier Bourgeois (2018), “Heat conduction measurements in ballistic 1d phonon waveguides indicate breakdown of the thermal conductance quantization,” *Nat. Commun.* **9**, 4287.
- Thomas, George, Jukka P. Pekola, and Dmitry S. Golubev (2019), “Photonic heat transport across a josephson junction,” *Phys. Rev. B* **100**, 094508.
- Tighe, T S, J. M. Worlock, and M. L. Roukes (1997), “Direct thermal conductance measurements on suspended monocrystalline nanostructures,” *Appl. Phys. Lett.* **70**, 2687.
- Timofeev, Andrey V, Meri Helle, Matthias Meschke, Mikko Möttönen, and Jukka P. Pekola (2009), “Electronic refrigeration at the quantum limit,” *Phys. Rev. Lett.* **102**, 200801.
- Tinkham, Michael (2004), *Introduction to Superconductivity*, 2nd ed. (Dover Publications).
- Wang, Haidong, Shiqian Hu, Koji Takahashi, Xing Zhang Hiroshi Takamatsu, and Jie Chen (2017), “Experimental study of thermal rectification in suspended monolayer graphene,” *Nat. Commun.* **8**, 15843.
- Wang, L B, O.-P. Saira, D. S. Golubev, and J. P. Pekola (2019), “Crossover between electron-phonon and boundary-resistance limits to thermal relaxation in copper films,” *Phys. Rev. Applied* **12**, 024051.
- van Wees, B J, H. van Houten, C. W. J. Beenakker, J. G. Williamson, L. P. Kouwenhoven, D. van der Marel, and C. T. Foxon (1988), “Quantized conductance of point contacts in a two-dimensional electron gas,” *Phys. Rev. Lett.* **60**, 848–850.
- Wellstood, F C, C. Urbina, and John Clarke (1994), “Hot-electron effects in metals,” *Phys. Rev. B* **49**, 5942–5955.
- Wharam, D A, T J Thornton, R Newbury, M Pepper, H Ahmed, J E F Frost, D G Hasko, D C Peacock, D A Ritchie, and G A C Jones (1988), “One-dimensional transport and the quantisation of the ballistic resistance,” *Journal of Physics C: Solid State Physics* **21** (8), L209–L214.
- Wu, Yong-Shi (1994), “Statistical distribution for generalized ideal gas of fractional-statistics particles,” *Phys. Rev. Lett.* **73**, 922–925.
- Yung, C S, D. R. Schmidt, and A. N. Cleland (2002), “Thermal conductance and electron-phonon coupling in mechanically suspended nanostructures,” *Appl. Phys. Lett.* **81**, 31.
- Zen, Nobuyuki, Tuomas A. Puurtinen, Tero J. Isotalo, Saumyadip Chaudhuri, and Ilari J. Maasilta (2014), “Engineering thermal conductance using a two-dimensional phononic crystal,” *Nat Commun* **5**, 3435.
- Zhan, Fei, Sergey Denisov, and Peter Hänggi (2013), “Power spectrum of electronic heat current fluctuations,” *Phys. Status Solidi B* **250** (11), 2355.
- Zhao, Erhai, Tomas Löfwander, and J. A. Sauls (2003), “Phase modulated thermal conductance of josephson weak links,” *Phys. Rev. Lett.* **91**, 077003.